Poly $_L$-lactic acid (PLLA) and Poly Methyl Methacrylate (PMMA) Blends and Their Interaction with CO_2 at Sub-Critical Conditions

By

Baisheng Yao

A thesis submitted to the

Faculty of Graduate Studies and Research

in partial fulfillment of the requirement

for the degree of

Master of Science

Carleton University

Department of Chemistry

1125 Colonel By Drive

Ottawa, Ontario, Canada

June, 2007

Your file Votre référence
ISBN: 978-0-494-33720-2
Our file Notre référence
ISBN: 978-0-494-33720-2

Abstract

This work demonstrated the possibility of processing blends of poly $_L$-lactic acid (PLLA) and poly methyl methacrylate (PMMA) with CO_2 through studying changes in the glass transition temperature, solubility, diffusivity and finally generated foam morphologies.

One glass transition temperature, Heat-induced crystallization and CO_2-induced crystallization were observed in the samples. However, the addition of PMMA to PLLA reduced the rate of PLLA crystallization and increased the decomposition temperature.

The solubility capacity for the blends was investigated. Analysis of the diffusion coefficients indicated them to be concentration dependent and therefore the possibility of existence of retrograde behavior in the blend-CO_2 system. The foam morphologies were strongly related to blend composition, foaming temperature, CO_2 saturation conditions as well as the CO_2 induced crystallization and retrograde behavior in the system.

A mathematical model was also implemented to predict CO_2 solubility, blend swelling factors and glass transition behaviors in blend-CO_2 system.

Acknowledgements

I am very glad to have had the opportunity to do my research and conduct my experimental work at the National Research Canada under the supervision of Dr. Victoria Nawaby. I thank her for her support, encouragement and sound advice. Her valuable questions, comments and suggestions eventually enabled me to grasp rich complexity and increased the value of this research greatly.

I would also like to express my most sincere thanks to Dr. Bob Burk and Dr. Liao Xia, Steve Liu, David Kinston, Gill Roberson and Dr. Pam Whitfield for their kind assistance in my research.

I wish to thank my entire extended families for providing a loving environment, understanding and support during the two years. My wife Chunqi Ma, my son Martin Yao, my mother-in-law Guilan Li and my father-in-law Shangzhi Ma were particularly supportive.

Finally I thank Carleton University for a Graduate Scholarship which gave me two years of financial support.

Table of Contents

List of Tables

List of Figures

Chapter 1

Introduction

1.1 Biopolymers

Many thermally stable and chemically stable polymers, such as polyethylene (PE), polyvinyl chloride (PVC), polystyrene (PS), Acrylonitrile-butadiene-styrene copolymer (ABS) are synthesized from fossil fuel and widely used as materials due to their outstanding chemical, physical and mechanical properties. However, billion tons of plastics disposed in the world per year have caused environmental concerns [1].

With limitation on oil resources and environmental issues, the polymer industry is seeking alternate source of raw materials and is therefore focusing on biological routes for resin production. As an alternative to conventional synthetic polymers, biopolymers can be used alone or combined with conventional plastics to reduce the widespread dependence on fossil fuels. Moreover, biopolymer will further contribute to reducing environmental pollution due to being biodegradable [2].

Biopolymers are generally naturally occurring polymers or synthetic polymers produced from renewable agricultural or biomass feedstock. Synthetic biopolymers offer greater advantages than natural biopolymers in that synthetic biopolymers can be tuned to give a wider range of properties in addition to having more available sources of raw materials. Biopolymers are susceptible to degradation in the presence of enzymes, bacteria, or other biological systems [3].

Polysaccharides, proteins, oils, fats, natural polyisoprenes, natural fibers are some examples of naturally occurring polymers. They are formed in natural environments during the life cycles of green plants, animals, bacteria and fungi. They are self-generating and also present in large quantities. The path of natural synthesis is extremely complex involving many different enzymes by complex metabolic processes. Biopolymers are also produced by vitro synthesis or chemical synthesis from renewable agricultural or biomass feedstock. For example, polylactic acid (PLA) is synthesized in chemical plants by polymerization from lactic acid that is produced from starch by a fermentation process [3, 4].

Biopolymers are used mainly as packing materials (carrier bags, wrappings, catering articles), consumer products (diapers, cosmetic articles, toys), agricultural tools (mulch films, planters) and medical devices (controlled drug delivery devices, orthopaedic and dental implants, cardiac pacemakers, sutures, artificial heart valves, and contact lenses). The general criteria for selecting a biopolymer for a specific application are to match the mechanical properties, the time of degradation and bio-compatibility in addition to ease in processing the material [5-7].

1.2 Poly L-Lactic Acid (PLLA) and Poly Methyl Methacrylate (PMMA)

1.2.1 Structure, Synthesis and Properties of PLLA

Poly Lactic Acid (PLA) is a well known biodegradable polyester which is increasing explored and studied in order to replace petroleum-based polymers [3]. PLA

is produced from lactide which is the cyclic dimer of lactic acid. Lactic acid and lactide are derived from natural source. The monomer for PLA is enantiomeric, having L- and D-isomers. PLAs synthesized from the L- isomers, D-isomers and racemic monomer are PLLA, Poly D-lactic acids (PDLA) and poly DL-lactic acid (PDLLA), respectively. Lactide also exists as two optical isomers; L-lactide is the naturally occurring isomer, and DL-lactide is the synthetic blend of D-lactide and L-lactide. The synthesis routes of PLA are presented in Figure 1.1 [8].

Physical properties of PLA are related to its stereosequence distribution. For example; pure PLLA has a faster rate of crystallization than PLA that is polymerized with most L-lactide and small amounts of either D-lactide or DL-lactide. Hence, the fraction of L-lactide in the PLA is linked to the crystallization properties of the polymer [8]. Both PLLA and PDLA are crystalline; exhibit high tensile strength and low elongation and consequently have a high modulus and slow degradation. PDLLA is amorphous in nature and exhibits a random distribution of both isomeric forms of lactic acid and accordingly is unable to arrange itself into an organized crystalline structure. PDLLA has lower tensile strength, higher elongation, and a much more rapid degradation [9]. PLLA shows melting (T_m) and glass transition (T_g) temperatures at approximately 180 °C and 63°C, respectively. The crystallization temperature (T_c) and T_m of PLLA decreases with decreasing L-lactate content in PLLA [10].

PLA is a biodegradable, bioresorbable polymer, which decomposes completely in a typical compost environment [3]. The degradation products of PLA promote plant growth and do not pose harm when used within the human body. Therefore; PLA is an

ideal material in biomedical applications, such as suture, capsule for controlled drug delivery systems and tissue engineering scaffolds [11].

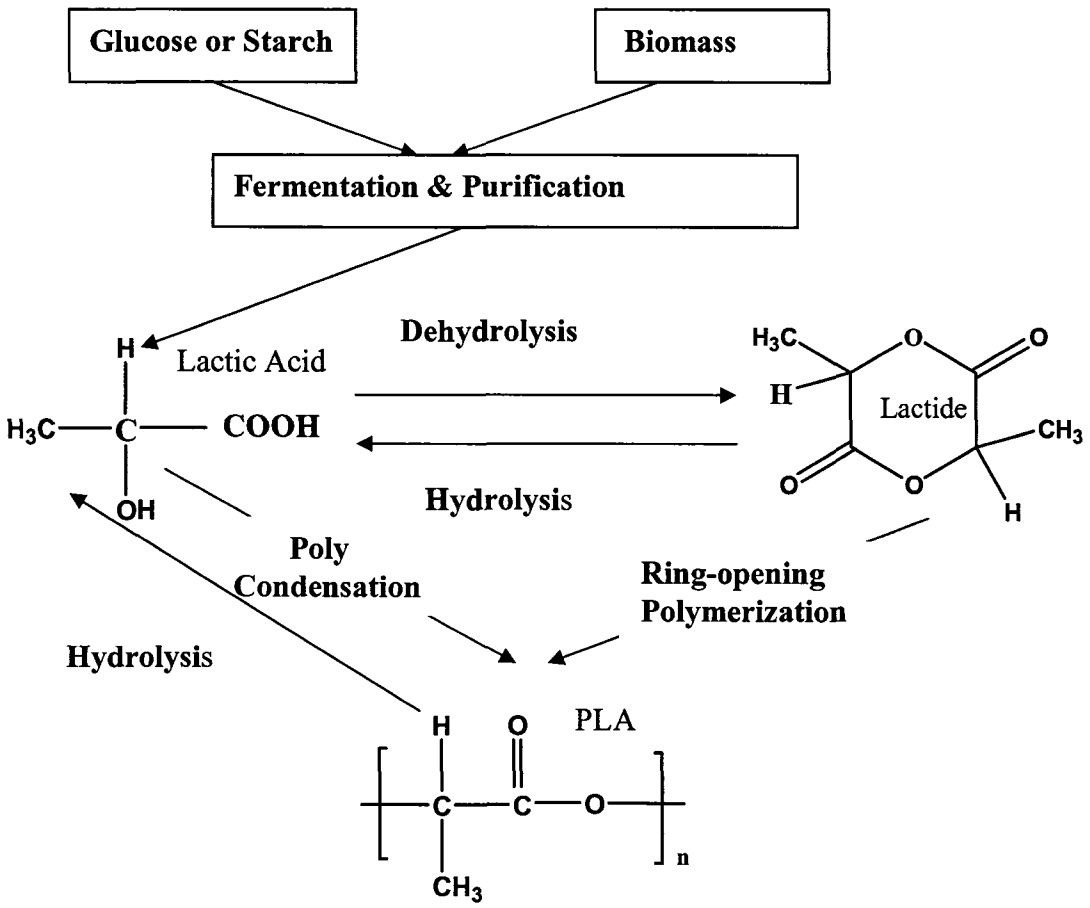

Figure1.1: synthesis routes of PLA [9].

Though thermal and mechanical properties of PLA are somewhat poor for use as ordinary structural materials, the environmental impacts and price reduction of bulk

production of PLA has made it a potential replacement for petroleum-based plastics like yard-waste bags, food containers, agricultural mulch films and etc [5, 6].

1.2.2 **Structure, Synthesis and Properties of PMMA**

PMMA is a petroleum-based polyester with outstanding mechanical, optical and biocompatible properties [12]. PMMA is an important class of petroleum-based thermoplastics which exist in three forms, atactic, isotactic and syndiotactic structure (Figure 1.2) [13].

PMMA is synthesized by free radical, anionic or group transfer polymerization from Methyl Methacrylate (MMA) which is produced from petrochemical industry. The T_g of syndiotactic PMMA is by as much as 60-70°C higher than that of isotactic PMMA. T_g of atactic PMMA with molecular weight around 100,000 is about 105°C. Stereoregularity and molecular weight of PMMA can be well controlled by anionic or group transfer polymerization with specific initiating systems and chain-end control [13-15].

Commercial PMMA is an amorphous, non-degradable, but biocompatible material with a higher thermal decomposition temperature in addition to having good structural gluing and polishing properties. PMMA has been widely used in auto and construction industries as plastic glass, as well as in dental and orthodontic applications [16, 17].

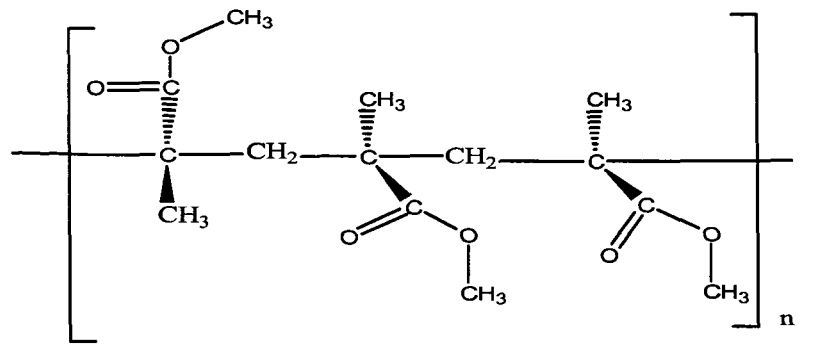

(a)

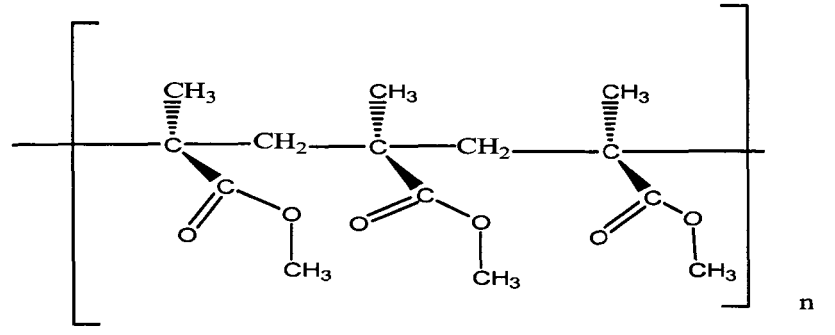

(b)

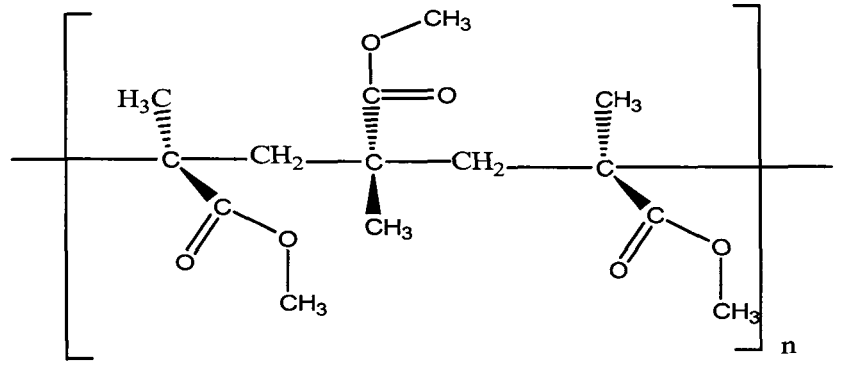

(c)

Figure1.2: The basic structure of the stereocomplex of (a) atactic PMMA, (b) isotactic PMMA, (c) syndiotactic PMMA [13].

1.2.3 Approved Applications of PLLA and PMMA by U. S. Food and Drug Administration (FDA)

PLA was approved in the 1960s by the FDA and since that time, products made from PLA, poly glycolic acid and their copolymers have been accepted for use as medical devices. PLA as a void filler following tooth extraction, orthopedic fixation devices and tissue-engineering scaffolds supplied by Atrix, Bionx W.L. Gore, Ethicon are approved by FDA and is currently available in the market [18].

PMMA was approved by FDA for use as contact lens, bone cement and implant materials. Contact lenses made by Lagado Corp (1992) and Lens Dynamics Inc(1992), bone cement made by Institute of Technical(2001) and Polymers Reconstructive A/S were approved by FDA in 1993 [19].

PLA blends such as PLLA/PDLLA, and PLLA blended with poly caprolactone (PCL), polyglycolic acid (PGA), and atactic poly [(R, S) –3-hydroxybutyrate] present distinct mechanical and biodegradation properties. The property adjustment through modification of components and blend ratio has the potential to extend the applications of this polymer even further in the biomedical industry [10,20].

1.3 Polymer Property Modification

Many polymers undergo treatments to modify their properties and extend their applications. These treatments include compounding, blending, foaming and stretching. Compared to chemical synthesis, physical treatments such as blending and foaming are more cost efficient.

This manuscript reports on the effect of blending two polymers and the physical property modification thus induced as a result of solubility of CO_2 in the matrix and formation of morphologies. Hence; we will give an overview on the blending process versus foaming of plastic with blowing agents.

1.3.1 Polymer Physical Properties

The polymer properties are divided into three interrelated categories: intrinsic, processing, and product properties [21]. Intrinsic properties refer to the properties of a substance which are reproducible in the lab. These include the density, melting temperature, optical and electromagnetic properties, as well as thermo physical and thermo chemical properties. Polymer properties related to processing include extrudability, mouldbility and stretchability. Product properties of polymer also called end-used properties are related to the material and product made from the polymers [1].

From the point of applications, the T_g is the most important single parameter and is a temperature range above which a brittle or tough polymer becomes rubbery. This parameter is affected by molecular properties (chain stiffness, intermolecular force) and controllable parameters (pressure, platicizers, molecular weight, copolymers, cross-linking, crystallinity, and tacticity). Increasing chain stiffness and intermolecular force raises the T_g of a polymer. Applying pressure to a polymer reduces its free volume and therefore increases the T_g [22]. This specific physical parameter in polymers therefore can be determined experimentally by means of Differential Scanning Calorimetry (DSC).

T_g is conventionally defined as the intersection of the straight line segments of the volume-temperature (v-T) or enthalpy-temperature (ΔH-T) plot. There are several

theories that propose to illustrate the glass transition phenomenon. The free volume theory states that the fractional free volume in polymer changes with temperature and hence the relationship is given by:

$$f_T = f_g + \alpha_f (T - T_g) \tag{1.1}$$

where; f_T and f_g are the fractional free volume at temperature T and T_g, respectively. The fractional free volume f is therefore defined as:

$$V_f/(V_0 + V_f) \approx V_f/V_0 \tag{1.2}$$

Where, V_0 and V_f are the occupied and the free volumes respectively, and α_f is the expansion coefficient [22]. The thermodynamic theory for T_g proposed by Gibbs and Di Marzio, which is based on the entropy of a polymer as a function of temperature is presented in section 1.5.1.3 in more detail since this theory will be used in this manuscript to develop the changes in T_g as a function of pressure.

1.3.2 Compounding Versus Blending

Properties of a polymer are closely related to its chemical structure such as stereoregularity, chain length and functional groups. Polymerization and co-polymerization are two basic means to produce a polymer with a specific chemical structure. In addition to the chemical structure, properties of a polymer are also related to crystallinity, its nature, and amount of additives. These factors influence almost all

properties of polymers, such as optical, electrical and mechanical as well as biological response [4].

Polymer blending is a technique to modify some of the properties of polymers. Melt mixing and solution mixing are two general methods and the properties of blends are dependent on the combination, composition and even the mixing process. Synthetic methods may not provide finely adjusted properties, but the blending methods can do. Furthermore, blending polymers is a more economical way of improving or changing properties than synthesizing new polymers [1, 4, 23].

1.4 Polymer Foams

Cellular plastics or foams are the expanded or sponge like plastics consisting of a minimum of two phases, a solid polymer matrix and a gaseous phase generated from a blowing agent. Formation of cellular plastics is yet another method of extending the applications of polymers. The foam features of polymers can improve mechanical properties, reduce material consumption, decrease dielectric constant and increase thermal insulation capability as well as enhancing light reflecting capabilities [24, 25].

Foams are industrially produced by extrusion and injection molding using blowing agents. There are two kind of blowing agent; physical blowing agent and chemical blowing agent. Foaming of polymers by either method involves generation of a gas in the matrix and upon inducing a thermodynamic instability in the polymer-gas solution therefore causing bubble nucleation and formation of a cellular or porous morphology. In the next section we will in detail describe the theoretical aspects of foaming.

1.4.1 Foaming: Theoretical Aspects

There are three steps to the process of gas foaming: gas dispersion, bubble growth and stabilization. Bubbles are formed as a result of the nucleation process in polymer-gas system. Nucleation in the foaming process induced either by heat or pressure change is divided into homogeneous or heterogeneous nucleation. If the bubbles are formed initially in a truly homogeneous manner, the nucleation process is called homogenous nucleation. Otherwise, bubble formation at the interface between a polymer and an additive is called heterogeneous nucleation. Bubbles form much easily during a heterogeneous nucleation process. Two equations are therefore commonly used, one for the rate of homogeneous nucleation (equation 1.3) and another for heterogeneous nucleation (equation 1.5).

$$N_0 = C_0 f_0 \exp(-\Delta G^*_{hom}/kT) \tag{1.3}$$

ΔG^*_{hom} is the homogeneous activation energy barrier, which is given by:

$$\Delta G^*_{hom} = (16\pi \gamma_{bp}) / (3\Delta P) \tag{1.4}$$

$$N_1 = C_1 f_1 \exp(-\Delta G^*_{hex}/kT) \tag{1.5}$$

ΔG^*_{hom} is the heterogeneous activation energy barrier, which is given by:

$$\Delta G^*_{hex} = (1/4)(16\pi \gamma_{bp}3) / (3\Delta P^2)(2+\cos\theta)(1-\cos\theta)^2 \tag{1.6}$$

In equation 1.3 through 1.6, C is the concentration of gas molecules, f is the frequency factor of molecules joining the nucleus, k is Boltzman's constant, T is the absolute temperature, γ_{bp} is the interfacial tension of the polymer-bubble interface, ΔP is the gas pressure, and θ is the contact angle of polymer-additive- gas interface [24, 26].

In foaming, bubbles are formed initially by nucleation and grow by diffusion of gas from the solution into the bubble. The gas pressure in the bubble is the driving force; the polymer inertia, viscosity and the interfacial tension of the bubble wall are the resistant against bubble growth [27] and bubbles tend to combine if given sufficient time. In the early stages bubbles are spherical in shape, but change to polyhedral shapes when fluid phase is insufficient. If the cell membranes surrounding a bubble are strong enough the bubbles will remain intact and the foams generated will have closed cells; if the membranes rupture, some of or all of cells will be open. However; extensive rupture before the foam is stabilized may lead to foam collapse. Finally, once the driving and resistant forces reach a balance, the cells stop growing and the system reaches a stabilized state whereby the foam matrix can be recovered [28, 29].

1.4.2 Foaming Techniques

General methods of producing thermoplastic foams involve thermal activation foaming (chemical blowing agent) or gas dissolution foaming (physical blowing agent) is involved. During thermal activation foaming, gases such as CO_2, N_2 and CO are released from the chemical blowing agents at elevated temperatures and therefore used to expand the matrix. In gas dissolution foaming, physical blowing agents such as CO_2, N_2,

propane, or pentane are injected into and mixed with a melted polymer. The system is then subjected to a sudden thermodynamic change either by releasing the pressure or changing the temperature of the polymer-gas solution. This sudden change results in the escape of the gas from the matrix leaving behind a porous structure [27, 30].

Conventional foaming techniques generally produce foams with cell size around $300\,\mu$m and cell densities around 10^6 cells/cm^3. Attempts have been made to generate foams with specific morphologies and cell sizes through addition of particulates (talc and salt). Salt leaching and freeze drying (phase separation) techniques have also been used to produce porous morphologies [30].

Particulate leaching involves the use of porogens. For example the water-soluble NaCl and hexane-soluble waxy hydrocarbons can be used as porogens. The porogens are first mixed with either a polymer at the melt state or added through a solution mixing process. Finally, the porogens are leached out by a porogon only soluble solution resulting in a foamed polymer with a much lower density than the starting resin. The porosity and pore size of the foams can be controlled by the amount of porogens and the size of the porogen particles, respectively. However, organic solvents used in the casting/particulate leaching procedure may preclude the possibility of adding pharmacological agents if the foams are for biomedical applications. The toxic residues left in the matrix may have a negative effect on the transplanted cells and active growth factors. The leaching step increases the foam preparation time; however the process has been reported to be suitable for prefabrication of cell-polymer constructs [31, 32].

Freeze drying techniques are used to create matrices for tissue engineering applications. The most common thermally-induced phase separation techniques are based

on the principle that the homogeneous polymer solution will convert to two phases due to the free energy change of mixing caused by the temperature change. The liquid–liquid phase separation or the solid-liquid phase separation takes place when the polymer solution is cooled down. After the solvent is removed, the fibrous matrices are formed [33, 34].

Traditionally CFC's and hydrocarbons were used as foaming agents, however due to tougher environmental regulations a more green solvent in processing of porous morphologies was sought. CO_2 has been a very successful physical blowing agent for foaming PMMA, PS, PET, polyurethanes (TPU) and various thermoplastic materials. Literature studies indicate detailed investigations on the effect of this gas at sub and supercitical states on the physical properties of the polymers and hence formation of voids and microcellular morphologies [35, 36].

1.4.3 Cellular Morphologies

Properties such as mechanical and thermal conductivity of foamed polymers are closely related to their cellular morphologies. Cell structures are characterized by cell size and distribution, cell shape, cell density, cell wall thickness, as well as being open or close cell.

The cell size can have a considerable influence on the properties of foamed plastics. For example; the coefficient of thermal conductivity of foams increases, when the cell size increases since there are more paths for heat transfer by radiation and convection. An increase in cell size also causes a rise in the Young's modulus of both flexible and rigid plastic foams. Cell sizes can be characterized by linear dimension (cell

diameter) or by the hydrodynamic radius which is equal to the ratio of the cross-sectional area of the cell to the perimeter of the cross section. The cell anisotropy of foamed polymer also affects foam strength, dielectric and mechanical properties [24].

An apparent density is another fundamental morphological parameter of foamed polymers which characterizes the relative contents of the solid and the gas phase in a material. The range of densities of foamed polymer is from 3 to 900 kg/m^3. Most of the physical properties of polymer foams are directly related to the densities.

Traditional industrial foaming processes produce foams with cell size larger than 0.25 mm. Foams with the cell size in the range of 1-100 μm and a cell density greater than 10^6 $cells/cm^3$ of the original solid material are called microcellular foams. Microcellular foams have attracted much attention due to their superior mechanical and thermal properties. The tensile strength of microcellular foams decreases in proportion to the foam density [37]. Thus foams with 50% relative density can be expected to have 50% of the strength of the solid polymer.

Solid-state batch and semi-continuous gas foaming process are the main processing methods to produce microcellular foams [38]. Depending on foam applications, the specifications on cell size and cell density of the cellular matrix change. For biomedical applications, foams designed for use as a substrate for cell growth and cell infiltration must have open and interconnected pores. For thermal and electrical insulation applications, layered foams are reported to be best suited [39, 40].

1.5 Supercritical CO_2 in Polymer Processing

CO_2 replacing chlorofluorocarbons (CFC) blowing agents has drawn much

attention in recent years due to the tunable properties of CO_2 and being and environmentally friendly solvent [41, 42]. Dissolution of CO_2 in many polymers not only results in plasticization, reduction of the T_g and subsequently creation of fine voids leading to cellular structures; but also in some cases induces crystallization in polymers. Nucleation and bubble growth are the basic mechanisms for gas foaming; CO_2 solubility, diffusivity, polymer properties, and the foaming conditions are other key factors in creating cellular morphologies with a wide range of porosities [43-46].

Application of high pressure CO_2 in foaming industry requires an accurate understanding of the interaction of CO_2 with a polymer such as mass transfer and plasticization. The interactions between the polymer and CO_2 are a thermodynamic rather than hydrostatic pressure effect. Strong interaction between the polymer and CO_2 enhances relaxation and mobility of the polymer chains and result in T_g depression [24]. This change in physical property therefore can be used to generate morphologies with unique characteristics. The porous morphologies generated therefore are dependent on amount of gas dissolved in the polymer and rates of diffusion. Gravimetric methods are normally used to determine the amount of dissolved gas. The sorption kinetic data can then be used and diffusion coefficients can be extracted by means of mathematical models.

1.5.1 Mathematical Models for Prediction of Gas Solubility, Gas Diffusion and Glass Transition

1.5.1.1 Gas Solubility in Polymers

The mass of CO_2 in polymer sample can be experimentally measured by a gravimetric method or predicted by mathematical models. In a gravimetric method the amount of gas uptake in the polymer is measured as a function of time at small pressures steps. A number of microbalances are commercially available and capable of carrying out such studies with a high degree of accuracy (10^{-6} g) in a wide pressure and temperature range. Nevertheless, gravimetric methods require the measurement or estimation of the swelling in the polymer phase as the result of gas dissolution in order to correct for buoyancy changes during the experiments [47].

Two models can then be used to determine the equilibrium solubility of the gas in the polymer. These are dual-mode sorption model and Sanchez-Lacombe equation of state describing the solubility of gases in polymers. Solubility of gases in a polymer may be carried out above or below its glass transition temperature. If sorption studies are performed in the glassy state (below the polymer's T_g), the dual-mode sorption model is suitable for the application and is given by the following equation:

$$S=k_H p + (S'_H b p)/(1+b p) \quad (1.7)$$

Where, S and p are the concentration and pressure of gas in the matrix. K_H, S'_H and b are the Henry's law constant , the Langmuir capacity and affinity factors, respectively [24, 43, 48].

Solubility of gases in polymers in the rubbery state, i.e. above its glass transition temperature can be modeled using the simple Henry's law model as described in the following equation 1.8:

$$S=k_H p \tag{1.8}$$

Where S, is the equilibrium solubility of the gas in the polymer, K_H is the Henry's law constant, and p is the gas pressure. Above the polymer's glass transition temperature Langmuirian sites no longer exist and therefore equation 1.7 reduces to equation 1.8. This equation has successfully predicted the solubility of gas in polymer at the rubbery state [43].

Determination of solubility of CO_2 in a polymer at various pressures can yield the solubility coefficient at each isotherm. Hence, the temperature dependence of gas solubility is described by a Van't Hoff relationship

$$S=S_0 exp(-\Delta H_s/RT) \tag{1.9}$$

Where S_0, ΔH_s, R, T are solubility pre-exponential factor, heat of sorption, universal gas constant and absolute temperature, respectively [49, 50].

A second equation used for determination of solubility of gases in polymers is Sanchez-Lacombe equation of state and is a widely used model to predict the solubility due to its well defined physical meaning and the available data. In this model, polymer-gas system is composed of mers and vacant sites (segments and holes). Density change resulting from dissolution of CO_2 is accommodated by the vacancies. The binary interaction parameter is only parameter required to describe the polymer-gas system

except the three molecular characteristic parameters of neat polymer and gas in this equation [51].

Using thermodynamic models plus advanced computing techniques to predict the properties of polymer-gas system can reduce experimental cost. Sanchez-Lacombe Equation, theories of solution equilibrium and Gibbs-Dimarzio criterion are used as the theoretical basis for calculation of the solubility and changes in the T_g of polymer-gas system.

Based on the mean-field theory, Isaac C. Sanchez and Robert H. Lacombe calculated the lattice energy of a system which is consists of segments and holes which are presented by lattice-fluid equation of state. The Sanchez-Lacombe equation of states (S-L EOS) has been widely used for calculating physical properties of polymers such as solubility, viscosity, T_g, etc. under high pressure CO_2 because of its applicability to both CO_2 and polymers [52, 53]. The S-L EOS is expressed as follows:

$$\tilde{\rho}^2 + \tilde{P} + \tilde{T}\left[\ln(1-\tilde{\rho}) + (1-\frac{1}{\gamma})\tilde{\rho}\right] = 0 \tag{1.10}$$

$\tilde{P}$, $\tilde{T}$ and $\tilde{\rho}$ are the reduced pressure, temperature, and density, respectively.

$$\tilde{P} = P/P^* \tag{1.11}$$

$$\tilde{T} = T/T^* \tag{1.12}$$

$$\tilde{\rho} = \rho/\rho^* \tag{1.13}$$

$$\gamma = P^* \upsilon^* / (R\,T^*) \tag{1.14}$$

$$\rho^* = m_w / (\gamma\,\upsilon^*) \cong m_w / \upsilon^* \tag{1.15}$$

ρ^*, P^*, T^* are characteristic parameters; R is gas constant, m_w is the average molecular weight and ρ^* is closed packed density which is equal to the crystal density. In Sanchez-Lacombe theory, $\tilde{\rho}^*, P^*,$ T* are derived from interaction energy ε^*, characteristic volume υ^* and the size parameter γ (number of lattice site occupied by a molecule); $(\gamma\,\upsilon^*)$ is closed packed molar volume of molecules [54, 55].

$$T^* = \varepsilon^* / R \tag{1.16}$$

$$P^* = \varepsilon^* / \upsilon^* \tag{1.17}$$

For pure component, characteristic parameters ρ^*, P^*, T^* can be determined by fitting experimental P-T-V data to equation (1.10) using an optimization procedure. γ, is the only dependent parameters which can be determined by fitting the equation $\gamma =$ P*υ^* / ($R\,T^*$).

For binary system:

$$\phi_i = \frac{m_i / \rho_i^*}{[m_1 / \rho_1^* + m_2 / \rho_2^*]} \tag{1.18}$$

$$\phi_i^0 = \frac{\phi_i}{\phi_1 + (\upsilon_1^* / \upsilon_2^*)\phi_2} \quad \textit{for } i=1 \textit{ and } 2 \tag{1.19}$$

$$\upsilon^* = \phi_1^0 \upsilon_1^* + \phi_2^0 \upsilon_2^* \tag{1.20}$$

$$\varepsilon^* = \phi_1^0 \varepsilon_1^* + \phi_2^0 \varepsilon_2^* - \phi_1^0 \phi_2^0 (\varepsilon_1^* + \varepsilon_2^* - 2\varepsilon_{12}^*) \tag{1.21}$$

$$\varepsilon_{12}^* = \varsigma_{12} (\varepsilon_1^* \varepsilon_2^*)^{1/2} \tag{1.22}$$

$$P^* = \varepsilon^* / \upsilon^* \tag{1.23}$$

$$T^* = P^* \upsilon^* / R = \varepsilon^* / R \tag{1.24}$$

$$1/\rho^* = m_1 / \rho_1^* + m_2 / \rho_2^* \tag{1.25}$$

Where; ε^* is the energy of creation of a vacancy in a binary mixture; ς_{12} is a binary interaction parameter; m_i ϕ_i and ϕ_i^0 are weight fraction, close-packed volume fraction and molar fraction of component i in the mixture, respectively.

The two phase equilibrium is defined by equating chemical potential of gas in the gas phase and polymer phase. For a special case of binary mixture of a semi-flexible polymer and a small molecule fluid (CO_2), the chemical potential of latter is noted as component 1 in pure state and is given by:

$$\mu_1^0/(R\,T) = \gamma_1\,[(-\tilde{\rho}_1 + \tilde{P}_1\,\upsilon_1)/\tilde{T}_1 + \upsilon_1((1-\tilde{\rho}_1)\ln(1-\tilde{\rho}_1) + \tilde{\rho}_1 \ln \tilde{\rho}_1/\gamma_1)] \qquad (1.26)$$

In the mixture, the chemical potential of CO_2 by lattice-fluid express:

$$\mu_1/(R\,T) = \ln \phi_1^0 + (1-\gamma_1/\gamma_2)\,\phi_2^0 + \gamma_1\,\tilde{\rho}\,\chi_{12}\,\phi_2^{0\,2} + \gamma_1\,[(-\tilde{\rho} + \tilde{P}_1\,\upsilon)/\tilde{T}_1 + \upsilon((1-\tilde{\rho})\ln(1-\tilde{\rho}) + \tilde{\rho}\ln\tilde{\rho}/\gamma_1))] \qquad (1.27)$$

$$\chi_{12} = (\varepsilon_1^* + \varepsilon_2^* - 2\varepsilon_{12}^*)/(R^*T) \qquad (1.28)$$

The condition of equilibrium between pure fluid and fluid dissolved in the polymer is $\mu_1^0 = \mu_1$. Generally, the P-T-V data of pure polymers and CO_2 are available in the literature. If the binary interaction parameter of a polymer - CO_2 system is known, the solubility of CO_2 can be calculated from equation 1.26, 1.27 and equation 1.10 through adjustment of ϕ_i^0. Conversely, from the P-T-V data or gravimetric measurements resulting in solubility of CO_2 in the polymer, the binary interaction parameter can be calculated.

1.5.1.2 Gas Diffusivity in Polymers

Classic Fick's Law (equation 1.29) describes the free diffusion of gas in a polymer and is given by [56, 57, 58]:

$$J = -D \frac{\partial C}{\partial x} \tag{1.29}$$

Where; J, D and $\frac{\partial C}{\partial x}$ are mass transfer flux, diffusion coefficient, and concentration gradient in mass transfer direction, respectively. When a polymer is exposed to CO_2 above its $T_{g,}$, classic Fick's Law can easily describe the mass transfer of the penetrant in the matrix [24]. However in cases whereby transport properties are being determined in a polymer below its T_g, the system is more complicated due to the interaction of gas with polymers resulting in plasticization, swelling, chain mobility and its results on relaxation time scale [59].

Several models are available to calculate gas diffusion coefficient in polymers through experimental sorption data. These are; half time, initial slope, moment methods and hybrid model. Half time method and initial slope model simply uses a few sorption data to calculate diffusion coefficient and therefore somewhat are poor in accuracy [56].

A model that successfully and reliably describes the diffusion of the gas in the polymer has been developed and published extensively. The well known nonlinear regression method (hybrid method) was proposed to solve for the gas diffusion in simple geometric polymer samples (films) [60]. The diffusion coefficients of CO_2 in many polymers and several temperature ranges have been deduced from the sorption kinetics data using this model as described by equations 1.3 through 1.34 respectively:

$$\frac{M_t}{M_\infty} = \phi(x) f(x) + ([1 - \phi(x)] g(x) \tag{1.30}$$

$$f(x) = \frac{4}{h}(\frac{Dt}{\pi})^{1/2} \tag{1.31}$$

$$g(x) = 1 - \frac{8}{\pi^2} \exp(\frac{\pi^2 Dt}{h^2}) \tag{1.32}$$

Where; D is diffusion coefficient; h is the thickness of film samples, $x = Dt/h^2$, M_t and M_∞ are the masses of gas sorbed at time t and $t = \infty$; $\phi(x)$ is the weighting function defined as:

$$\phi(x) = 1, \; x \leq 0.05326 \tag{1.33}$$

$$\phi(x) = 0, \; x \succ 0.05326 \tag{1.34}$$

Although there are a number of models available for determination of diffusion coefficients in polymers, the hybrid model has obvious advantages. This model only requires sorption data. The uncoupled values of D and M_∞ can be determined whereas other models do not allow for this and thus the values are coupled.

Through sorption kinetic studies and use of the Hybrid model diffusion coefficient of the gas in a polymer can be studied at various temperatures. Therefore,

activation energy for diffusion in the material can be found by the following equation [56]:

$$D=D_0 \exp(-\Delta H_D/RT) \quad (1.35)$$

Where D_0, ΔH_D, R, T are diffusion pre-exponential factor, activation energy for diffusion, universal gas constant and absolute temperature, respectively; D_0 is temperature independent constant and ΔH_D is pressure independent.

1.5.1.3 Glass Transition for Polymer-Gas System

T_g of polymers can be calculated by using Gibbs-Dimarzio theory which assumes the entropy of the mixture to be equal to zero at the T_g. The entropy S of the mixture is given [61, 62]:

$$\frac{-S}{\gamma NR} = (\upsilon-1)\ln(1-\tilde{\rho}) + \ln\tilde{\rho}/\gamma_1 + (\phi_1/\gamma_1)\ln(\phi_1/\gamma_1) + (\phi_2/\gamma_2)\ln(\phi_2/\gamma_2) + 1 +$$

$$(\ln(2/Z)-1)/\gamma + (\phi_1/\gamma_1)(\gamma_1-2)[\ln(1-f_1) - f_1\Delta\varepsilon_1/(RT) + (\phi_2/\gamma_2)(\gamma_2-2)[\ln(1-f_2) -$$

$$f_2\Delta\varepsilon_2/(RT)] \quad (1.31)$$

Where; N is the number of molecules in a system; Z- coordination number of the lattice; $\Delta\varepsilon_i$ is the increase in intramolecular energy that accompanies the "flexing" of a bond in a type i chain; f_i represents the equilibrium number of flexed bonds given by

$$f_i = \frac{(Z-2)\exp(\Delta\varepsilon_i/(RT))}{1+(Z-2)\exp(\Delta\varepsilon_i/(RT))} \tag{1.32}$$

$\Delta\varepsilon_i$ for CO_2 is equal 0. For example Z was chose as10 for studies on the PMMA-CO_2 system [63]. T_g may be calculated by solving the group equations 1.10, condition of equilibrium of solubility equations 1.26 & 1.27, and equation 1.31 simultaneously.

1.5.2 CO_2-induced crystallization in polymers

Polymers can either exist as amorphous or semicrystalline and rates of crystallization can be varied by changes in temperature, annealing and quenching of the samples. The change in ordering of the macromolecule is achieved by controlling the temperature and changes to the rate of molecular relaxations. An alternative method of inducing relaxation in polymers is by dissolving gases in polymers and changing the free volume in the samples. Gases have been reported to be able to cause crystallization in polymers. As an example CO_2-induced crystallization has reported in poly ethylene terephthalate (PET), poly ether ether ketone (PEEK), Polypropylene (PP) and PLLA [64 - 66]. The rate of crystallization in most polymers typically follows a scaled exponential rate law that was first proposed by Avrami:

$$X_t = 1\text{-}exp\ (-kt^n) \tag{1.33}$$

Where; X_t is the weight fraction of the polymer crystallized at time t; k is the kinetic constant and n is Avrami exponent [67].

The overall crystallization rate is controlled by nucleation rate or the crystal growth rate. When the temperature is lower than the temperature of maximum crystallization rate; (T_{max}) is the equilibrium melt temperature, where, T_m presents the melt temperature of a polymer.

.

$$T_{max} \cong (T_g+T_m)/2 \tag{1.34}$$

Dissolution of CO_2 will accelerate the crystallization rate of semicrystalline polymer within the crystallization growth region [24]. Since this gas is capable of either inducing crystallization in some amorphous polymers and also affects rates of crystallization in semicrystalline polymers corrections must be applied to the sorption data. Gas sorption and diffusion only occur in amorphous phase in a semicrystlline polymer; the crystalline part acts as a barrier for gas diffusion. The volume fraction of amorphous part in a semcrystlline polymer can be determined by XRD or DSC studies and further used to correct the sorption data. The solubility for amorphous part can be calculated by [56]:

$$S_a = S_0/\varphi_a \tag{1.35}$$

Where; φ_a is the volume fraction of amorphous phase, S_0 is the apparent solubility and S_a is solubility coefficient in amorphous phase. The diffusion coefficient also can be described by [56]:

$$D_a = D_0 \tau \beta \tag{1.36}$$

Where; D_0 is observed diffusion coefficient; τ is a geometric tortuosity parameter related to the distance between crystallites, and β is the chain immobilization factor. If the value of τ or β is not available, equation 1.36 can be approximated as:

$$D_a = D_0 / \varphi_a \tag{1.37}$$

1.6 Interaction of CO_2 with PLLA

The solubility and coefficient of CO_2 in poly lactic acid (PLA) were measured at temperatures from 313.2k to 463.2k and pressure up to 10 MPa; the solubility data were corrected for amorphous region of PLA and correlated with the Sanchez and Lacombe equation of state [68]. The sorption kinetics, solubility, diffusion and crystallization behaviors were also studied at 25°C and pressure up to 5.5 MPa; the time dependence of CO_2-induced crystallization and higher solubility of CO_2 in PLLA were found. Stretched cell in the core and partial interconnected cell with diameter 100-600 nm in the skin were reported in this study [69]. The authors suggested that high solubility of CO_2 in PLLA was due to specific interactions of gas with the carbonyl group in PLLA and the sharp increase in diffusion coefficient may be due to transitions from glassy to the rubbery state. Furthermore, CO_2-induced crystallization in PLLA was found to effect foaming and the type of foam morphology in the samples. Using a high-pressure DSC indicates the crystallization kinetic constant was dependent on crystallization temperature and

concentration of CO_2 in PLLA [70]. Attempts thus far made to improve mechanical properties and cellular morphologies in PLLA resulted in preparing PLLA nanocomposites. Nanocomposite is a material created by introducing nanoparticulates into a macroscopic material and in the case of PLLA due to effect of the gas on the polymer major improvements were not obtained. The nanocomposite samples did not produce fine cellular morphology when compared to neat PLA and clay agglomeration resulted in uneven cellular morphology when samples were treated with sub-critical CO_2 [71].

1.7 Interaction of CO_2 with PMMA

Strong interaction between PMMA and CO_2 enhances dissolution of CO_2 in the matrix and T_g depression [72,73]. At temperatures well below T_g, the solubility of CO_2 in PMMA is convex toward pressure (Flory-Huggin's type), but becomes linear against pressure at higher temperature (Henry's type)[49].

Interaction of CO_2 with PMMA in a wide temperature range has been studies and the diffusion coefficient of the gas as a function of pressure has been found to increase sharply below T_g, and to show a linear relationship above T_g (Figure 1.3). This dramatic change was also found in sorption kinetic data and such change in both sorption kinetics and diffusion caused by CO_2 is an indication of a phase change in the polymer (from glassy to rubbery state) [49, 61, 74].

The relationship between T_g and the gas pressure (p) the polymer is in equilibrium with, gives information on the extent of plasticization and changes in the thermal transitions. In most polymer–gas systems the T_g–p relationship follows a linear path;

however, in certain polymer–gas systems with favorable interaction between molecules, a retrograde path was observed, and subsequently two transitions were detected under a constant gas pressure [49].

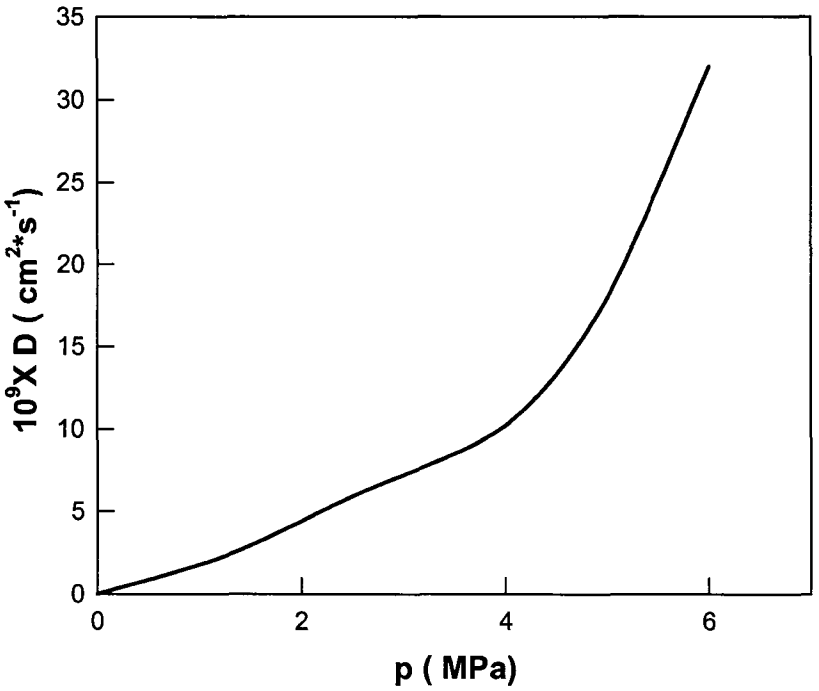

Figure1.3: Diffusion coefficient of CO_2 in PMMA at 25°C [49].

The retrograde vitrification phenomenon in PMMA-CO_2 was found by high pressure thermal analysis and predicted by a model that was based on lattice theory and the Gibbs-Di Marzio criterion [49, 63, 70, 75]. Two glass transition temperatures (T_g) exist in the vicinity of the critical point of CO_2. One is normally expected plasticized T_g; another corresponds to the rubber to glass transition that is also called retrograde vitrification. The retrograde vitrification results from rapid lost of CO_2 on heating. For example, PMMA is in the rubbery state when saturated with CO_2 at 0°C and 3.4 MPa (Figure 1.4). When the system is heated to 5°C under a constant gas pressure 3.4 MPa, a

rubber to glass transition occurs and therefore foams obtained will be very different in morphology. Moreover; on continued heating, a phase change from glassy to rubbery state will occurs [75]. The existence of the rubbery state at low temperatures was used to generate ultramicrocellular foams with average cell size of 0.35 um and cell density 4.4×1013 cell·g^{-1} at a low-temperature foaming [49, 74].

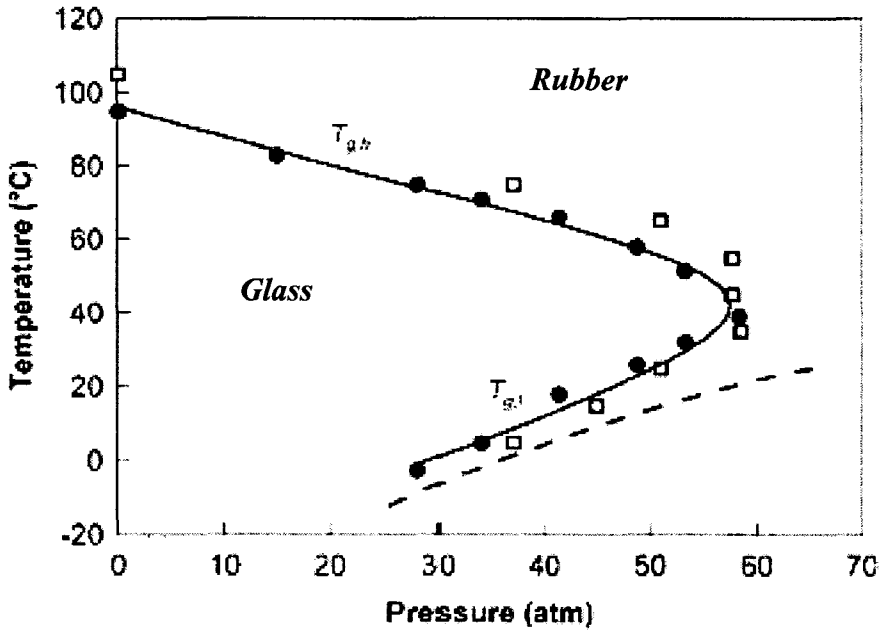

Figure1.4: Retrograde vitrification in PMMA-CO_2 system [62]

1.8 Research Objectives

Blending of the two polymers without phase separation not only has economic advantages, but also results in potential improvements on the mechanical properties of polymers. Furthermore, formation of CO_2 blown cellular plastics is another method of extending the application of polymers while being cost effective. To date most studies published in the field of polymer–CO_2 foams has been on neat petrochemical resins. A

very limited number of publications are available on interaction of CO_2 with biopolymers. Of the cases presented on biopolymer-CO_2 systems fundamental data is still somewhat scarce. A thorough examination of the literature also indicates very few cases involving CO_2 foaming of polymer blends which involves mixtures of petrochemical base resins. Furthermore, limited information on fundamental changes of the polymer blends in contact with the gas and hence foam morphologies are presented.

CO_2 solubility and foaming of a polymer blend consisting of a petrochemical base PMMA and a bio–based polymer such as PLLA, to the best of our knowledge is not available. Both polymers in the neat form with CO_2 have been studied and morphologies with very interesting properties have been produced. As such; this study reports on CO_2 sorption, diffusion and morphological change of PLLA/PMMA blends at sub-critical conditions. The relationship between cell structure of CO_2 blowing foams and properties changed by CO_2 and blending has been exploited and presented.

Mathematical methods as presented will be used in predication of sorption kinetic data and changes in the T_g of the polymer as a function of pressure. Furthermore, a numerical model developed by Condo and Johnston has been used and developed in the prediction of the data for blend-CO_2 system instead of neat polymer-CO_2 system.

References

1. Kolybaba, M. A.; Tabil, L.G.; Panigrahi, S.A. Recent Development in the Biopolymer Industry, *North Central ASAE/CSAE Conference (Canada)* **2004**, Paper Number: MB04-301

2 . Robert, W.; Lenz, J. M. S. *Pure Appl. Chem.* **1995**, A 32 (4), 797-803.

3. Domb, A. J. *Polymeric site-specific Pharmacotherapy*, John Wiley & Sons Ltd: England, **1994**, 1-45.

4 . Seymour, R. B.; Carraher Jr., C. E. *Polymer Chemistry , 3rd ed.*, Marcel Dekker Inc.: New York, **1992**, 155-184, 487-488.

5 . Munene, C. N.; Kampen, W. H.; Njapau, H. *Journal of the Science of Food and Agriculture* **2002**, 82 (3), 309-314.

6. Gross, R. A.; Kalra, B. *Science* **2002**, 297, 803-808.

7. Warth, H.; Muelhaupt, R.; Schaetzle, J. *Journal of Applied Polymer Science* **1997**, 64 (2), 231-242.

8. Thakur, K. A. M.; Kean, R. T. ; Hall, E. S.; Kolstad, J. J.; Lindgren, T. A. ; Doscotch, M. A. J.; Siepmann, I.; Munson, E. J. *Macromolecules* **1997**, 30, 2422-2428.

9. Metha, R; Kumar, V.; Bhunia, H.; Upadhyay, S. N. *Journal of Macromolecular Science: Part C: Polymer Reviews* **2005**, 45, 325–349.

10. Lu, L.; Mikos, A. G. *Polymer Data Handbook* **1999**, 627-633.

11. Hoffman, A. S; Schoen F. J.; Lemons, J. E.; Ratner, B. D.(eds) *An Introduction to Materials in Medicine*, Academic Press: New York, **1996**, 356—360.

12 . Zhang, G.; Zhang, J.; Wang S.; Shen, D. *Journal of Polymer Science: Part B: Polymer Physics* **2002**, 41, 23-30.

13. Liquori, A. M. ; Anzuino, G. ; Coiro, V.M.; D'Alagni, M. Stantis, P. D.; Savino, M. *Nature* **1965**, 206, 358-362.

14. Zeng, W. R.; Li, S. F.; CHOW, W. K. *Journal of Fire Sciences* **2002**, 20, 401-433.

15. Jiang, G. J.; Hwu, J. M. *Journal of Polymer Science: Part A: Polymer Chemistry* **2000**, 38, 1184-1194.

16.Tretinnikov, O. N. *Macromol. Symp.* **2003**, 203, 57-69.

17. Nodono, M.; Makino T.; Nishida, K. Reactive & Functional Polymers 2003, 57, 157–161.

18. Middleton, J.; Tipton A. *Biomaterials* **2000**, 21, 2335-2346.

19. U. S. Food and Drug Administration, *CDRH Databases*, Code of Federal Regulations: 886.3027, 886.1385.

20. Zhang, L.; Xiong, C.; Deng, X. *Journal of Applied Polymer Science* **1995**, 56, 103-112.

21. Krevelen, D.; Hoftyzer, P. *Properties of Polymers, 2nd ed.*, Elsevier Scientific Publishing Company: Amsterdam-Oxford-New York, **1976**, 4-7, 475-503.

22. Mark, J. E.; Eisenberg, A.; Graessley, W.W.; Mandelkern, L.; Samulski, E. T.; Koenig, J. L.; Wignall, G. D. *Physical Properties of Polymers, 2nd ed.*, America Chemical Society: USA, **1993**.

23. Al-Saigh, Z. Y. Int. J. *Polym. Anal. Charact.*, **1997**, 3, 249-291.

24. Klempner, D.; Frisch K. C. (editors) *Handbook of Polymeric Foams and Foam Technology,* Oxford University Press: New York, **1991,** 10-30.

25. Itoh, M.; Kabumoto, *A. Furukawa Review*, **2005**, 28, 32-38.

26. Colton, J.S. and Suh, N.P. *Polymer Engineering and Science* **1987**, 27, 485-492.

27. Lee, S. T. *Foam Extrusion Principal & Practice*, CRC Press: New York, **2000**, 35- 65.

28. Goel, S. K.; Beckman, E. J. *Polymer Engineering and Science* **1994**. 34, 1148-1156.

29. Goel, S. K. *Polymer Engineering and Science* **1994**, 34, 1137-1147.

30. Manniene A. Gas Transport Phenomenon and Foamability of CO_2-PMMA Nanocomposite System, *Master Thesis of University of Ottawa* **2004,** 90-102.

31 . Karageorgiou,V.; Karageorgiou, Kaplan,D. *Biomaterials*, **2005**, 27, 5474-5491.

32. Mikos, A. G.; Temenoff, J. S. *Electronic Journal of Biotechnology* **2000**, 3, 114-119.

33 . Schugens, Ch.; Maquet, V.; Grandfils, Ch.; Jerome, R.; Teyssie, Ph. *Journal of Biomedical Materials Research* **1996**, 30, 449-461.

34. Yoon Sung Nam, Tae Gwan Park, *Biomaterials* **1999**, 20 1783-1790.

35. Michaeli , W.; Heinz, R. *Macromolecular Materials and Engineering* **2001**, 284-285, 35 – 39.

36. Kemmere, M. F.; Meyer, T. (editors) *Supercritical Carbon Dioxide in Polymer Reaction Engineering*, WILEY-VCH Verlag GmbH & Co.: Germany, **2005**, 215-217.

37. Kumar, V.; VenderWel, M.; Keller, J. E.; Seeler, K. A. *Journal of Engineering Materials and Technology* **1994**, 116, 439-445.

38 . Kumar, V.; Schirmer, H.G. Proceeding of SPE Antec 95, Bostoon, USA, 1995, 2, 2189-2193.

39. Kim, T. K.; Yoon, J. J.; Lee, D. S.; Park, T. G. *Biomaterials* **2006**, 27, 152-160.

40. Handa, Y. P.; Zhang, Z. *Cellular Polymers* **2000**, 19, 77-90.

41. Cooper, A. I. *Advanced Materials* **2003**, 15, 1049-1059.

42 . Kazarian, S. G. *Macromol. Symp.* **2002**, 84, 215-228.

43 . Tomasko, D. L.; Li, H.; Liu, D.; Han, X.; Wingert, M. J.; Lee L. J.; Koelling, K. W. *Ind. Eng. Chem. Res.* **2003**, 42, 6431-6438.

44. Xu, Q.; Ren, X.; Chang, Y.; Wang, J.; Yu L.; Dean, K. *Journal of Applied Polymer Science* **2004**, 94, 593-597.

45. Shieh, Y. T.; Liu, K. H.; Lin, T. L. *Supercritical Fluids* **2004**, 24, 101-112.

46. Cotugno, S.; Maio, E. D.; Mensitieri, G. *Ind. Eng. Chem. Res.* **2005**, 44, 1795-1803.

47. Zhang, Y.; Gangwani, K.K.; Lemert, R. M. *Journal of Supercritical Fluids* **1997**, 11, 115-134.

48. Vieth, W. R. ; Howell , J. M.; Hsieh, J. H. *Journal of Membrane Science* **1976**, 1, 177-220.

49. Handa, Y. P.; Zhang, Z.; Wong B. *Cellular Polymers* **2001**, 20, 1-16.

50. Zimmerman, C. M.; Koros, W.J. *Polymer* **1999**, 40, 5655-5664.

51. Sanchez, I. C.; Lacombe, R. H. *The journal of Physical Chemistry* **1976**, 80, 2352-2362.

52 . Naffakh, M.; Gomez, M.A.; Ellis, G.; Marco C. *Polymer Engineering and Science* **2006**, 36, 1411-1418.

53. Condo, P.D.; Sanchez, I. C.; Panayiotou, C.G.; Johnston, K.P. *Macromolecules* **1992**, 25, 6119-6127.

54. Garg, A.; Gulari, E. ; Manke, C. W. *Macromolecules* **1994** ,27, 5643-5653.

55. Areerat, S.; Hayata ;Y.; Katsumoto, R.; Kegasawa T.; Egami, H.; , Ohshima M. *Journal of Applied Polymer Science* **2002**, 86, , 282–288.

56. Navaby, A. V.; Zhang, Z.; Lee, S. T.(editor); Gendron R. (editor) *Polymer Foam Series-Thermoplastic Foam Processing Principle and Development*, CRC Press: USA, **2005**, 1-25.

57. Ying, Y. G. *The Research Methods for Heterogeneous Catalyst (Chinese)*, Chemical Industry Press: Beijing, **1988**, 1-160, 223-236.

58. Wong, B.; Zhang, Z.; Handa, Y. P. *Journal of Polymer Science: Part B: Polymer Physics* **1998**, 36, 2025-2032.

59. Zhang, Y.; Gangwani, K.K.; Lemert, R. M. *Journal of Supercritical Fluids* **1997**, 11, 115-134.

60. Balik, C. M. *Macromolecules* **1996**, 29, 3025-3029.

61. Liu, D.; Li, H.; Noon M. S.; Tomasko, D. L. *Macromolecules* **2005**, 38, 4416-4424.

62. Handa, Y. P.; Zhang, Z. *Journal of Polymer Science: Part B: Polymer Physics* **2000**, 38, 716-725.

63. Condo, P.D.; Sanchez, I. C.; Panayiotou, C.G.; Johnston, K.P. *Macromolecules* **1992**, 25, 6119-6127.

64. Mizoguchi, K.; Hirose, T.; Kamiya, Y. *Polymer* **1987**, 28, 1298-1302.

65. Naffakh, M.; Gomez, M.A.; Ellis, G. and Marco C. *Polymer Engineering and Science* **2006**, 36, 1411-1418.

66. Tajada,M. ; Tanigaki, M.; Ohshima, M. *Polymer Engineering and Science* **2001**, 41, 1938-1946.

67. Avrami, M. J. *Chem. Phys.* **1941**, 9, 177-182.

68. Sato, Y.; Yamane, M.; Sorakubo, A.; Takishima, S.; Masuoka, H; Yamamoto, H.; Takasugi M. *The 21st Japan Symposium on Thermophsical Properties*, Nagoya, Japan, **2000**, 196-199.

69. Liao, X.; Nawaby, A. V.; Day, M. *ACS* **2005**, Washington, USA.

70. Takada, M.; Hasegawa, S.; Ohshima, M. *Polymer Engineering and Science* **2004**, 44, 186-196.

71. X. Hu, A.V. Nawaby. H. E. Naguib, M. Day, X. Liao, *ANTEC*, **2005**, Boston, USA.

72. Handa, Y.P.; Kruus, P.; O'' Neill, M. *Journal of Polymer Science: part B: Polymer Physics* **1996**, 34, 2635-2639.

73. Condo, P.D.; Johnson, K.P. *Macromolecules* **1994,** 27, 365-371.

74. Zhang, Y.; Gangwani, K.K. and Lemert, R. M. *Journal of Supercritical Fluids* **1997**, 11, 115-134.

75. Takahashi, M.; Yamamoto, Y.; Nawaby A. V.; Handa, Y. P. *Journal of Polymer Science: part B: Polymer Physics* **2003,** 41, 2214-2217.

Chapter 2

Experimental

2.1 Introduction

This chapter provides a detailed description of the experimental equipment and procedures used in collecting information on interaction of PLLA/PMMA blends with CO_2 gas. All experiments were carried out on equipment available at the Institute for Chemical Process and Environmental Technology at the National Research Council of Canada. Specific properties of the blends were then determined from the experimental data using established a well published methods.

2.2 Sample Preparation

2.2.1 Materials

PMMA in pellet form (M_w= 108,500, M_n =56,700, T_g =106.7°C, and density=1.27 g/cm^3) was supplied by Canus Plastics. PLLA polymer in pellet form (M_w= 63,366, M_n =32754, T_g =54.1°C, T_m =165.8°C, and density=1.18 g/cm^3) was supplied by Unitika Polymer Inc., Japan. Bone dry CO_2 (99% pure) supplied by air products was used. Since PLLA is sensitive to moisture in air, samples were kept under vacuum until used.

2.2.2 Melt Blending

A Minlab microcompounder (Thermo HAAKE Rheomex CTW5) was used for preparation of the blends. Samples were weighted in order to prepare blends in the

composition 25/75, 50/50 and 75/25 wt% PLLA/PMMA ratrios. Samples in pellet form were feed through a hopper into the microcompounder and mixed at 200°C. Polymer samples were melt-mixed at 200°C while being circulated for 2 minutes in the chamber before extruding the rods.

2.2.3 Compression Molding

Since sorption kinetic studies required samples in film form the extruded rods where then compression molded at 200°C. Samples were pressed into discs with diameter 13.5 mm and thickness of 0.37 mm at 200°C followed by quenching them in ice water. The entire process took 5 minutes and samples for sorption, foaming and thermal analysis were prepared by this method using prefabricated molds.

2.3 Blend Characterization

2.3.1 Differential Scanning Calorimetry (DSC)

Differential Scanning Calorimetry (DSC) measures the heat flow between a sample and a reference. The heat flow and temperature of the sample are monitored and compared to a reference material or blank measuring pan. The amount of energy absorbed (endotherm) or evolved (exotherm) as the sample undergoes a physical change (eg melting, crystallization, glass transition) is measured in calories as a function of the temperature change. [1].

The thermal history of blend samples were tested using DSC 2920, TA instruments Inc. This instrument was calibrated using mercury, water and indium as reference material. During the experimental studies, sample in the form of discs with

weight in the range of 5 mg-10 mg were loaded in aluminum pans and were sealed using a special press available from TA instruments. Samples were heated from 30 to 200°C at a heating rate of 5°C /min under a Nitrogen (N_2) environment with a flow rate of 50 mL/min.

In order to study the morphological change induced by heat, samples were analyzed when quenched from melt to yield an amorphous structure. Blend samples after being quenched in ice water were also annealed at 90°C and different time intervals in order to investigate the rate of crystallization as a function of time. All experimental runs were carried out under the above heating rate and environment. The % crystallinity in polymers can be obtained through the following equation [1]:

$$\% \, crystallinity = \frac{\Delta H}{\Delta H^0} \tag{2.1}$$

where, ΔH is the heat of fusion of semicrystalline samples and ΔH^0 is the heat of fusion of 100% crystalline samples which is 146 kJ/mol for PLLA [2]. For PLLA/PMMA blends, ΔH^0 is proximately calculated by ΔH^0 of 100% crystalline PLLA multiplied by weight percent of PLLA in blends.

Since CO_2 is capable of crystallizing some polymers, each blend sample in the amorphous state was treated with CO_2 under different saturation conditions of pressure and temperature for 24 hours and subsequently analyzed by DSC. The data was then compared to untreated samples either by heat or dissolution of CO_2 and extent in crystallization was studied through evolution of peaks and changes in peak shapes.

Since both heat and CO_2 are capable of crystallizing PLLA, the crystal content in the samples induced by CO_2 was further studied using x-ray diffraction patterns. This step therefore ensured that the crystal content being measured in the samples was as a result of CO_2 only and not heating the sample.

2.3.2 Thermo gravimetric Analysis (TGA)

Thermo Gravimetric Analysis (TGA) measures weight changes in a material as a function of temperature (or time) under a controlled atmosphere. TGA studies are commonly used to measure a material's thermal stability and composition. Weight changes observed at specific temperatures correlate to volatilization of the sample's components, decomposition, oxidation / reduction reactions, or other changes [1].

AutoTGA 2950 (TA Instruments) was used to test the weight change of blends and the neat polymers in air (60 ml/min). Compression molded samples with weight about 10mg were used and heated from 30 to 500°C at a heating rate of 10°C /min. In order to investigate the decomposition rate of blends at different temperature, the isothermal conditions between 150°C with 350°C were also chosen to study the weight changes as a function of time. The investigations were carried out using the same experimental steps for the neat polymers and results were compared to the blend samples. The decomposition rates of blends were calculated by equation:

$$r = \frac{dw}{wdt} \tag{2.2}$$

where; w and t are the weight of the sample and the process time respectively; r is the decomposition rate.

2.3.3 X-ray Diffraction (XRD)

X-ray diffraction (XRD) is used to determine the crystal structure and degree of crystallinity in polymers. Bragg's law is the theory basis of XRD, which is defined as:

$$2d \sin\Theta = n\lambda \tag{2.3}$$

Where; λ is wavelength of radiation, Θ is the angle of diffraction and d is a line of atoms of spacing.

By Bragg's law and miller indices (h, k, l), the crystal structure of a polymer can be determined. But, polymers are never 100% crystalline since the stereochemistry is never perfect. In most cases obtained XRD pattern from a polymer is reflections of several microcrystals with different orientation [3]. However this information is sufficient enough to determine the crystalline content in the polymer samples. The degree or % crystallinity is determined by comparing the relative area under the crystalline peaks to that of amorphous scatter from a 1-dimensional XRD pattern. The % crystallinity (X_c) can then be calculated using formula:

$$X_c = (A_c / A_{total}) * 100 \tag{2.4}$$

where; A_{total} is the intensity total area under peak for the sample containing crystal and amorphous parts. A_c is intensity or the area for the crystalline part and is defined as [3]:

$$A_c = A_{total} - A_{amorphous} \quad (2.5)$$

The samples in the form of discs with diameter 13.5 mm and thickness of 0.37 mm were studied for changes in morphological characteristics when treated with in CO_2 at 0 and 25°C at various pressures for 24 hours, and then compared to neat polymer films. Treated samples were aged for 1 week at 25°C before each test. All films were characterized by XRD (Bruker AXS Inc.) using CoK_α and a 2D HISTAR detector at a radiation wavelength of 1.5418 Å, and a scan range of 2θ from 1 to 40° with a scan speed of 0.9° / minute.

2.4 CO_2 Sorption Kinetic Study

A microelectronic balance was used to measure mass changes in the polymer as a function of time when placed in contact with CO_2 at 0 and 25°C. This in-situ gravimetric method provides a convenient and accurate method for measuring the kinetics of absorption and the equilibrium solubility of gas in the polymer. The balance and control system is presented in figure 2.1 [4, 5].

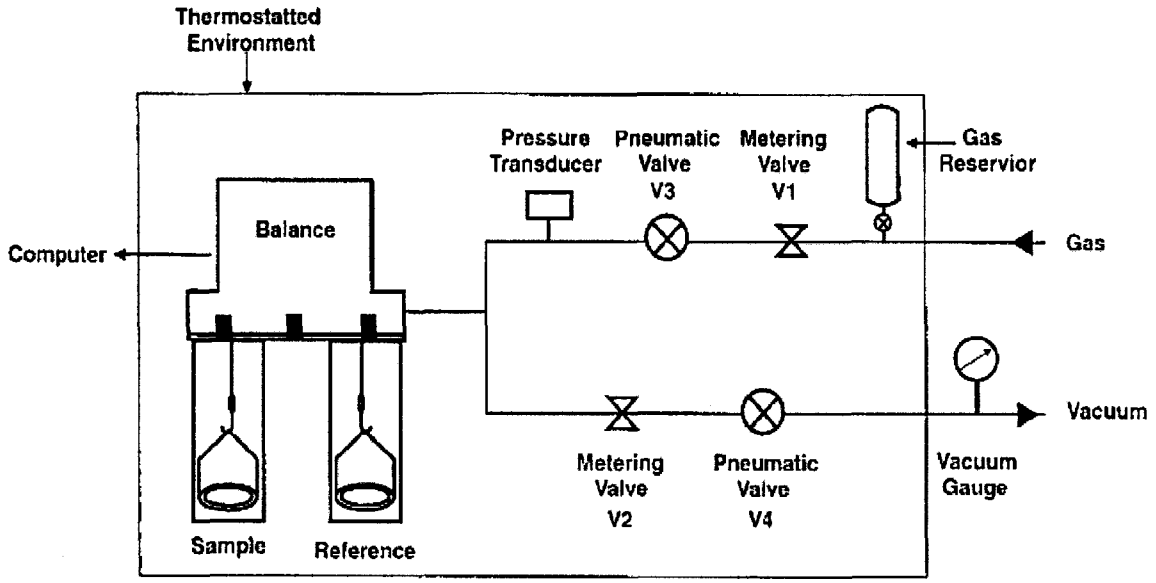

Figure 2.1: A schematic of the gas handling and control system (Handa at al. [5])

Approximately 0.3–0.5 g of each sample was placed in the balance and degassed for 48 hours. A maximum pressure of 3.4 and 5.5 MPa were used for studies at 0 and 25 °C, respectively. The chosen maximum pressures ensured processing the samples with gaseous CO_2. Prior to each sorption run, CO_2 gas was preheated to the experimental temperature and sorption steps at various pressures and constant temperatures of 0 and 25°C were carried out. The change in the polymer mass as a result of gas uptake was recorded as a function of time (every 10 seconds). A period of 24 hours was required for the system to reach equilibrium and to obtain the final amount of gas uptake in the polymer. Blank runs under the same experimental conditions provided the balance zero–shift as a function of pressure and mass readings were thus corrected. Since a small volume difference between the sample and reference side in the balance develops as a

result of gas dissolution in the polymer and hence matrix dilation, buoyancy corrections were applied to the solubility data. The corrected solubility is given by [4, 5]:

$$S=\frac{w_a + w_b}{m_p} \tag{2.6}$$

where; S is the corrected solubility of gas in the polymer; m_p is mass of a polymer sample, w_a is the apparent mass gain after correction for zero shift of balance. w_b is buoyant factor defined as:

$$w_b = \rho_g(\Delta V_i + \Delta V_d) \tag{2.7}$$

where; ρ_g is density of gas (CO_2) determined from the IUPAC tables of fluid state. ΔV_i is the volume difference between the sample and reference at beginning; ΔV_d is the volume change of the polymer due to dilatation as a result of gas sorption.

2.5 Foaming Studies

2.5.1 Sample Preparation

Polymer blend samples in the form of discs with diameter 13.5 mm and thickness of 0.37 mm were placed in a pressure vessel and saturated with CO_2 in the sub-critical region (A maximum pressure of 3.4 and 5.5 MPa was used for studies at 0 and 25 °C respectively). Samples were soaked for 24 hours at 25°C and 0°C respectively to ensure equilibrium was reached in the system. The pressure of the vessel was then quickly

released and the samples were placed in a water bath for 30 seconds in the range 50-90°C. Samples where quickly transferred to an ice bath to arrest the morphology.

A rapid pressure drop and temperature change will result in bubble nucleation due to state of super-saturation and is followed by bubble growth followed by freezing the morphology. In this process along with bubbles growth, the gas concentration in the polymer drops which results in increasing the effective T_g of the polymer increased resulting in a cellular morphology [6].

2.5.2 Foam Characterization

All specimens were characterized for density and structural properties using the total immersion method and field emission scanning electron microscope (SEM) respectively. The SEM uses a beam of highly energetic electrons to examine objects on a very fine scale [3].

A Jeol JSM-840A SEM operating at 15 kV acceleration voltages was used to examine the morphology and cell structure of PLLA/PMMA foams. The SEM images were processed by means of ImageJ software and cell sizes and cell densities were obtained.

The cell densities were determined by counting the number of cell on SEM photos. The number of pores per cubic micrometer can be estimated by:

$$N_f = (n\, M^2/A)^{3/2} \tag{2.8}$$

where n is the number of celles on micrograph; M is the amplification; A is the area of the micrograph and N_f is the cell density [7].

Foam densities were determined by weighing the samples in air and water using an analytic balance (Mettler AE163). The foam densities ρ_f were the determined using the following equation:

$$\rho_f = w_{air} * \rho_{water} / (w_{air} - w_{water}) \quad (2.9)$$

where ρ_{air} is the density of air and ρ_{water} is the densities of water; w_{air} and w_{water} are the apparent weights of a foam in air and water respectively.

References

1 . Wendlandt, W. W. *Thermal Analysis (3th edition)*, Wiley-Interscience: New York, **1986**, 9-80,213-269.

2. Lu, L. and Mikos, A. G. Poly (Lactic acid), *Polymer Data Handbook*, **1999**, 627-633, Oxford University Press Inc., New York

3. Ying, Y. G. *The Research Methods for Heterogeneous Catalyst (Chinese)*, Chemical Industry Press: Beijing, **1988**, 134-160, 223-236.

4.Wong, B.; Zhang, Z.; Handa, Y. P. *Journal of Polymer Science: Part B: Polymer Physics*,**1998**, 36, 2025-2032.

5. Handa, Y. P.; Zhang, Z.; Wong, B. *Cellular Polymer* **2001**, 20, 1-16.

6 . Singh, L.; Kumar, V.and Ratner, B.D. *Biomaterials* **2004**, 25, 2611-2617.

7. Kumar, V. and Weller, J. *Journal of Engineering for Industry* **1994**, 116, 413-421.

Chapter 3

Results and Discussions

3.1 PLLA/PMMA Blend Characterization

Although there are many reported studies in the literature on formation of single phase blends in polymers, their interaction with gases has been mainly looked at in terms of permeations studies. Very limited studies are available in the area of CO_2 foaming of polymer blends. Of the reported cases the polymer blends have been prepared from a combination of two polymers derived from petrochemical based resins. A few combinations of polymer blends exhibit miscibility and good interaction between the components. For example, Poly Ethylene Oxide (PEO)/PMMA and Polystyrene (PS)/ Poly Vinyl Methyl Ether (PVME) are two polymers which form a miscible and a one phase blend. Other polymer combinations forming a miscible blend are Syndiotactic Polystyrene / PS and isotactic PMMA /PMMA where their interactions with CO_2 have also been presented in the literature and unique morphologies were generated [1-3].

A recent investigation has demonstrated that PLLA/PMMA blends form a single phase and miscible blend. Samples processed by different processing methods indicated that the properties of the blends varied based on the processing technique that was chosen. Miscibility and phase behavior of PLLA/PMMA blends prepared by solution/precipitation, solution/casting, melt mixing and reactive blending are reported. Phase separation was observed to occur in samples prepared by the solution/precipitation

method, however; samples prepared by solution/casting did not exhibit phase separation [4-6]. Hence to extend the applications of PLLA; blending without phase separation offers many opportunities for this polymer thus far not reported in the literature. Blending with PMMA therefore can result in potential improvements on the properties of PLLA due to improved mechanical and optical properties of PMMA [7].

3.1.1 DSC Analysis

Thermal analysis performed on the prepared PLLA/PMMA blend samples in this study revealed the 75/25 wt% sample to be semicrystalline in nature and amorphous for 50/50 and 25/75 wt% compositions (Figure 3.1).

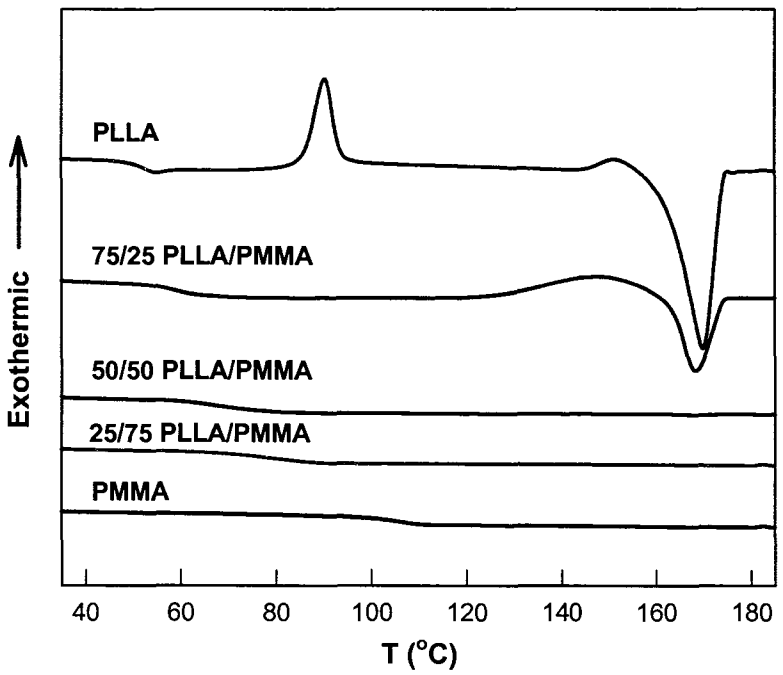

Figure 3.1: DSC thermograms of neat and polymer blend samples.

The neat and blend polymers exhibited one T_g; values of which are presented in Table 3.1. In addition, % crystallinity in the samples as well as the crystalline melt points is also presented in this table. Neat PLLA polymer underwent cold crystallization at 90°C; however no recrystallization of this polymer was observed in the blends of 50/50 and 25/75 wt% composition.

The heat of fusion (ΔH) of semicrystalline PLLA and PLLA/PMMA blend in 75/25 wt% was obtained by integration of the melting peaks on DSC thermograms. With addition of higher concentrations of PMMA to PLLA; the recrystallization behavior in PLLA was considerably affected. Table 3.1 provides the value for heat of fusion of 100% crystalline PLLA as presented in the literature and the value is compared to the value obtained for the 75/25 wt% sample [1]. The % crystallinity (Table 3.1) was obtained by dividing the heat of fusion for the tested samples by heat of fusion of 100% crystalline PLLA sample.

Table 3.1: Thermal transition of the neat and polymer blend samples.

Polymer Sample	Tg (°C)	Tm (°C)	ΔH(J/ g)	Crystallinity (%)
PLLA	54.1	170.1	32.7	37.6
PLLA/PMMA 75/25 wt %	58.9	168.2	2.0	2.3
PLLA/PMMA 50/50 wt %	66.6			
PLLA/PMMA 25/75 wt %	85.1			
PMMA	106.7			

Effect of temperature on the blend samples and possible morphological changes

were also investigated. Annealing the blends at 90°C for different time intervals resulted in recrystallization to occur in the PLLA/PMMA 50/50 and 75/25 wt% samples. With an increase in annealing time, an increase in crystalline content was observed. After 24 hours the % crystallinity in the 50/50 wt% PLLA/PMMA blend reached 19 % as compared to 38 % found in the neat PLLA sample (Figure 3.2).

Upon quenching PLLA from melt, amorphous samples were obtained and the matrix fully recrystallized after 45 minutes at 90°C. Therefore, nearly all PLLA portion of the 50/50 wt% blend sample crystallized upon annealing, however; the rate of recrystallization was much slower than neat PLLA.

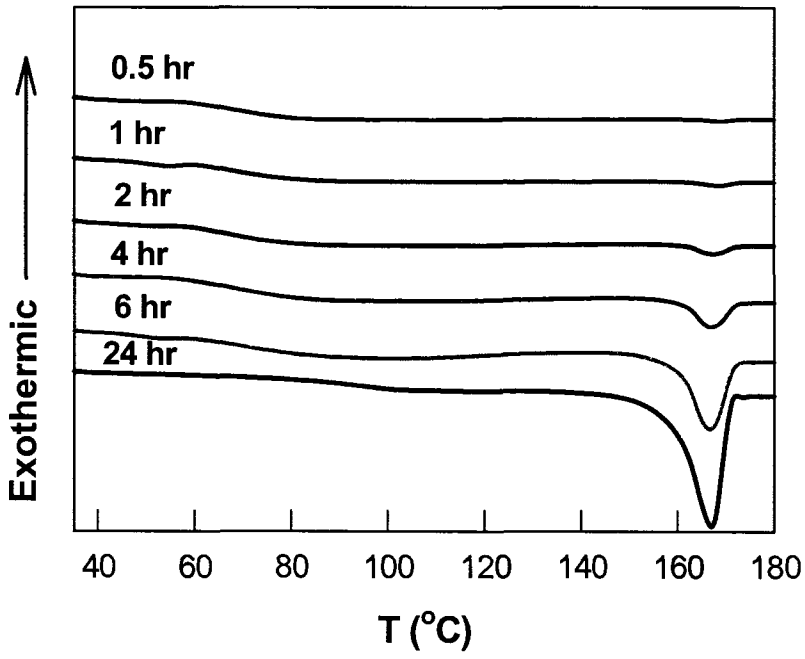

Figure 3.2: DSC thermograms PLLA/PMMA 50/50 wt %, annealed at 90°C.

Annealing also resulted in the glass transition temperature to increase for blends as a result of changes in the amorphous volume fraction in the polymer.. . Table 3.2 provides information on the changes of glass transition temperature as a function of annealing time. Samples annealed for 24 hours reached a T_g of 78.5 °C which is an almost 18°C increase as compared to the Tg (54.1 °C) of the neat polymer.

Table 3.2: Thermal transition for PLLA/PMMA 50/50wt% samples after annealing.

Annealing time (hr)	0	0.5	1.0	2.0	4.0	6.0	24.0
T_g (°C)	66.6	66.6	66.7	67.1	68.6	71.0	78.5

3.1.2 TGA Analysis

The thermal stability of blends in air was investigated by means of TGA. The temperature at which a 1% weight loss was observed was therefore chosen as initiation of the decomposition process. With an increase in PMMA content, the PLLA decomposition temperature increased thus allowing for this polymer to be thermally stable at much higher temperatures (Figure 3.3).

The decomposition properties of blends are related to neat polymers and the interaction between them [8, 9]. PLLA thermally decomposes at 148.5°C, however; when present with PMMA in the ratio of 75/25 wt% the decomposition temperature increases to 222.1°C (Figure 3.3).

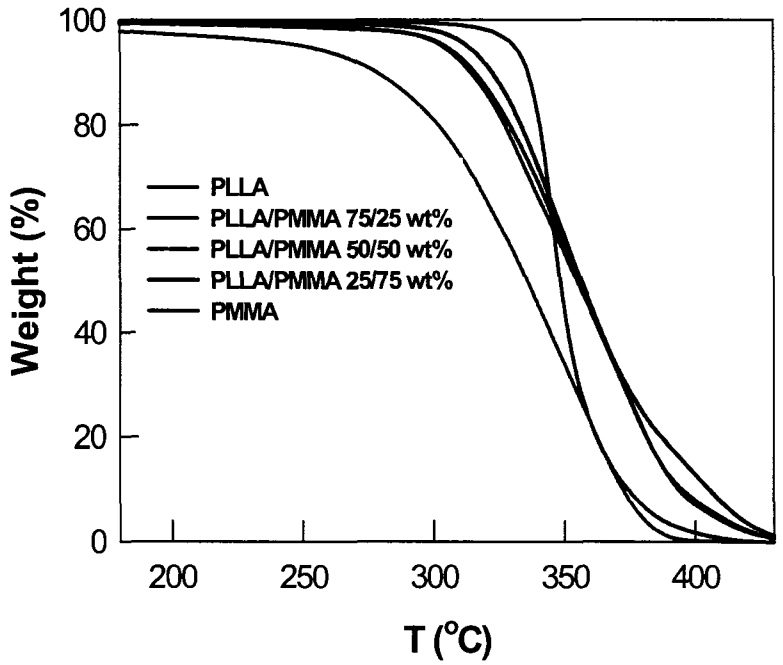

Figure 3.3: TGA thermograms of neat and polymer blend samples in air.

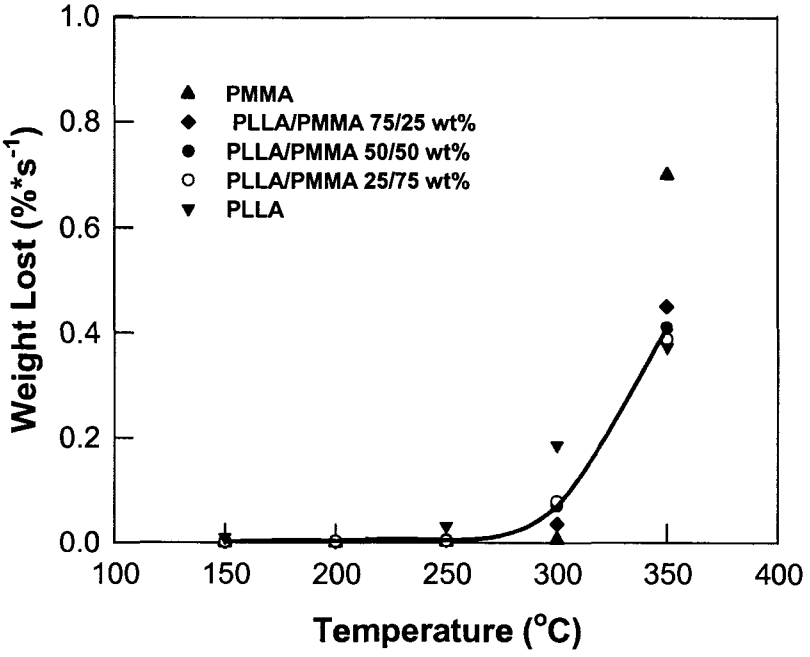

Figure 3.4: Weight loss rates of the neat and polymer blends in air. Curve is drawn through to show trend in data.

The decomposition rates of blends were calculated at 150, 200, 250, 300 and 350°C respectively by equation 2.2 as described in Chapter 2, section 2.2.2. The results are presented in Figure 3.4.

The decomposition rates of blends and neat PLA polymer remained less changed at temperatures below 250°C and increased rapidly above this temperature. With an increase in PMMA content in the blends the decomposition temperature increased to about 300°C whereby a sharp increase in the decomposition curve is observed after 250°C (Figure 3.4). Furthermore; it was difficult to identify more than one decomposition stage in the TGA thermograms for the tested samples (Figure 3.3). The decomposition data for neat and blend samples overlap and follow a similar trend as expected.

3.2 Sorption Kinetics, Solubility and Diffusion Coefficient

The solubility of CO_2 in the neat polymers were measured with the same gravimetric equipment used in this study and has been reported in the literature. As such data obtained on the sorption of this gas in the tested blend samples has been compared to those of the neat polymers available at 0 and 25°C.

The solubility of CO_2 at 0 and 25°C in a 50/50 wt% blend of PLLA/PMMA is presented in Figure 3.5 and as observed with an increase in the saturation pressure the sorption became faster as the polymer became more plasticized.

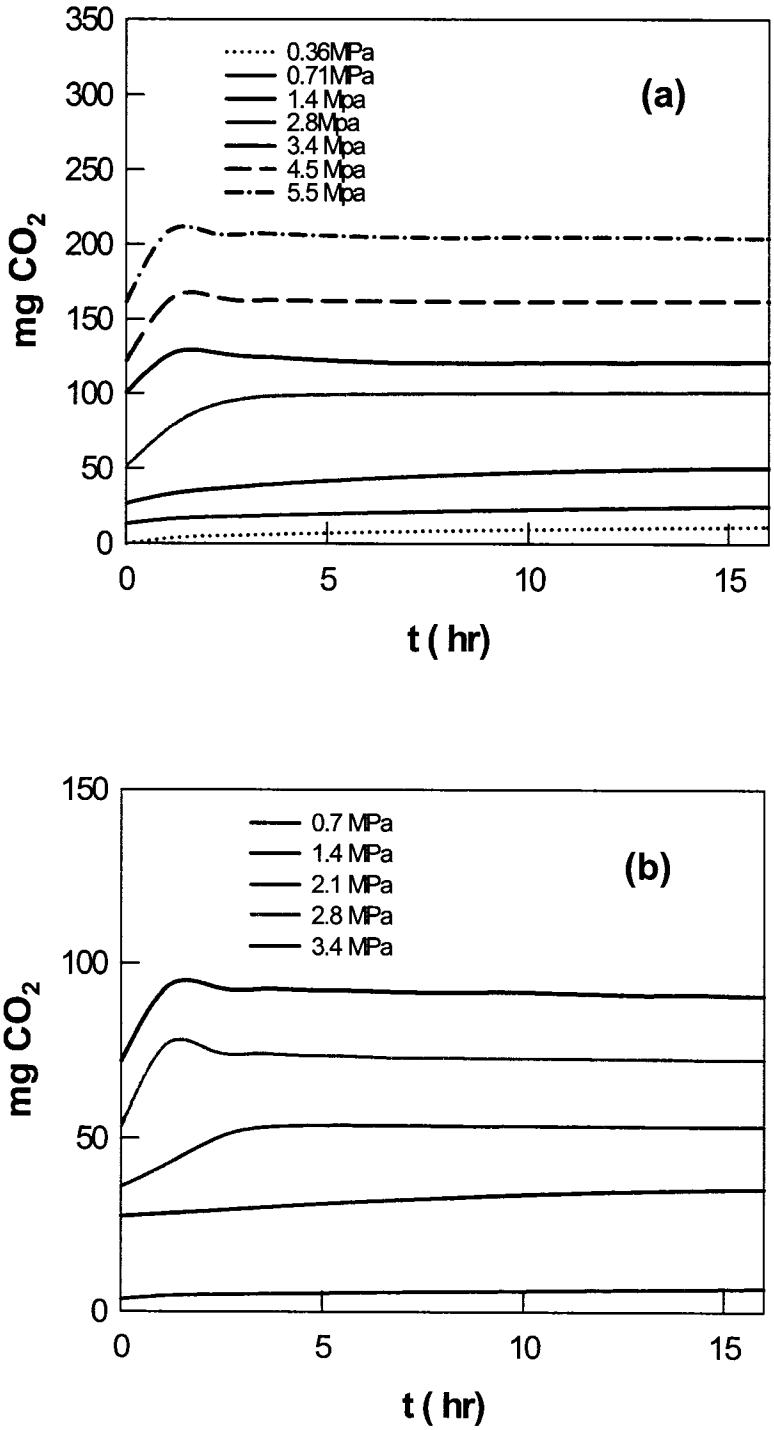

Figure 3.5: Sorption kinetics of CO_2 in 50/50 wt% PLLA/PMMA blend: (a) 25°C and (b) 0°C.

At a maximum pressure of 5.5 MPa, the sorption curve exhibits a small knee similar to the ones observed for PLLA–CO_2 and PET–CO_2 systems, indicating gas induced crystallization in the polymer. The developed knee was associated with the formation of ordered domains in the polymer and therefore rejection of the gas from the matrix [10-12]. The pressure at which the knee is first observed was noted to be at about 3.4 MPa.

The equilibrium solubility of CO_2 in the blend samples is presented in Figure 3.6 and compared to those obtained for the neat polymers. The solubility capacity for the 25/75, 50/50 and 75/25 wt% PLLA/PMMA blend is very similar to neat PMMA with PLLA exhibiting a higher CO_2 uptake. While the equilibrium solubility of CO_2 in the 50/50 and 75/25 wt% sample at 0°C is similar to that at 25°C, the CO_2 pressures resulting in such solubility levels are much lower.

As expected the solubility of CO_2 in blends increases with an increase in pressure. With a decrease in temperature the solubility of the gas in the polymer increases at much lower pressure and as such a higher Henry's law constant is observed. The same trend in the solubility coefficient is also observed for the neat polymers.

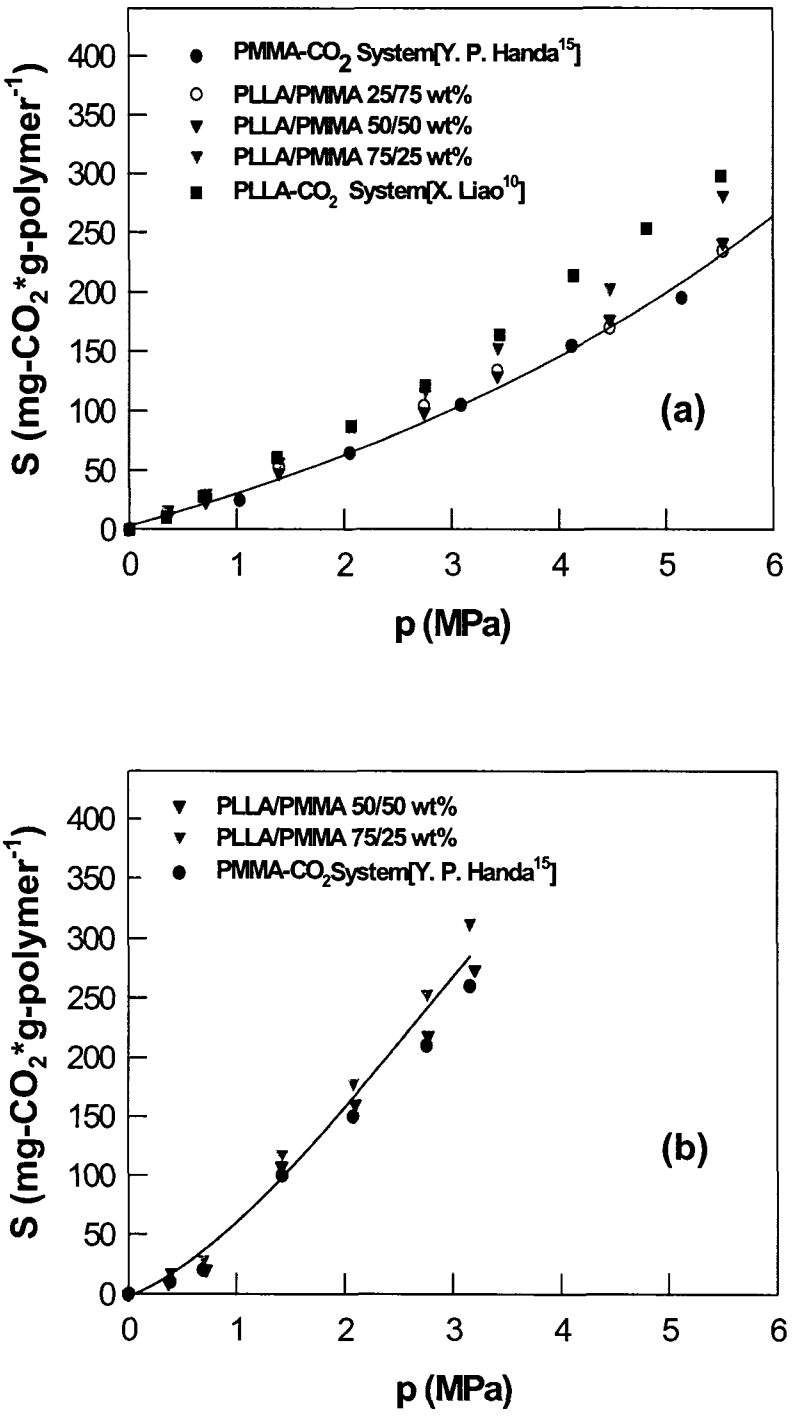

Figure 3.6: Equilibrium solubility of CO_2 in blends; (a) 25°C and (b) 0°C in 50/50 and 75/25 wt% blend samples. Curves are drawn through to show trend in data.

Table 3.3: Henry's Law Constant for CO_2 in neat and polymer blends.

Polymer Sample	K_H (mg CO_2*g polymer $^{-1}$*MPa $^{-1}$) (25°C)	K_H (mg CO_2*g polymer $^{-1}$*MPa $^{-1}$) (0°C)
PMMA [Handa et al. [15]]	39.0	76.3
PLLA/PMMA 25/75 wt %	40.6	
PLLA/PMMA 50/50 wt %	42.3	79.6
PLLA/PMMA 75/25 wt %	48.7	91.6
PLLA [Liao et al. [10]]	54.1	

The values for Henry's law constant of CO_2 at 0 and 25°C in the blend samples is presented in Table 3.2. These values were obtained from the dual sorption model (equation 1.7) as presented in Chapter 1. The data is compared to those obtained for the neat polymers in the tested temperature range. With an increase in PLLA content in the blends, an increase in the Henry's law constant was observed at each isotherm due to an increase in the free volume created in the polymer as a result of blending. The increase in free volume in samples can also be observed through DSC data and a shift in the T_g of the blend samples to lower temperature.

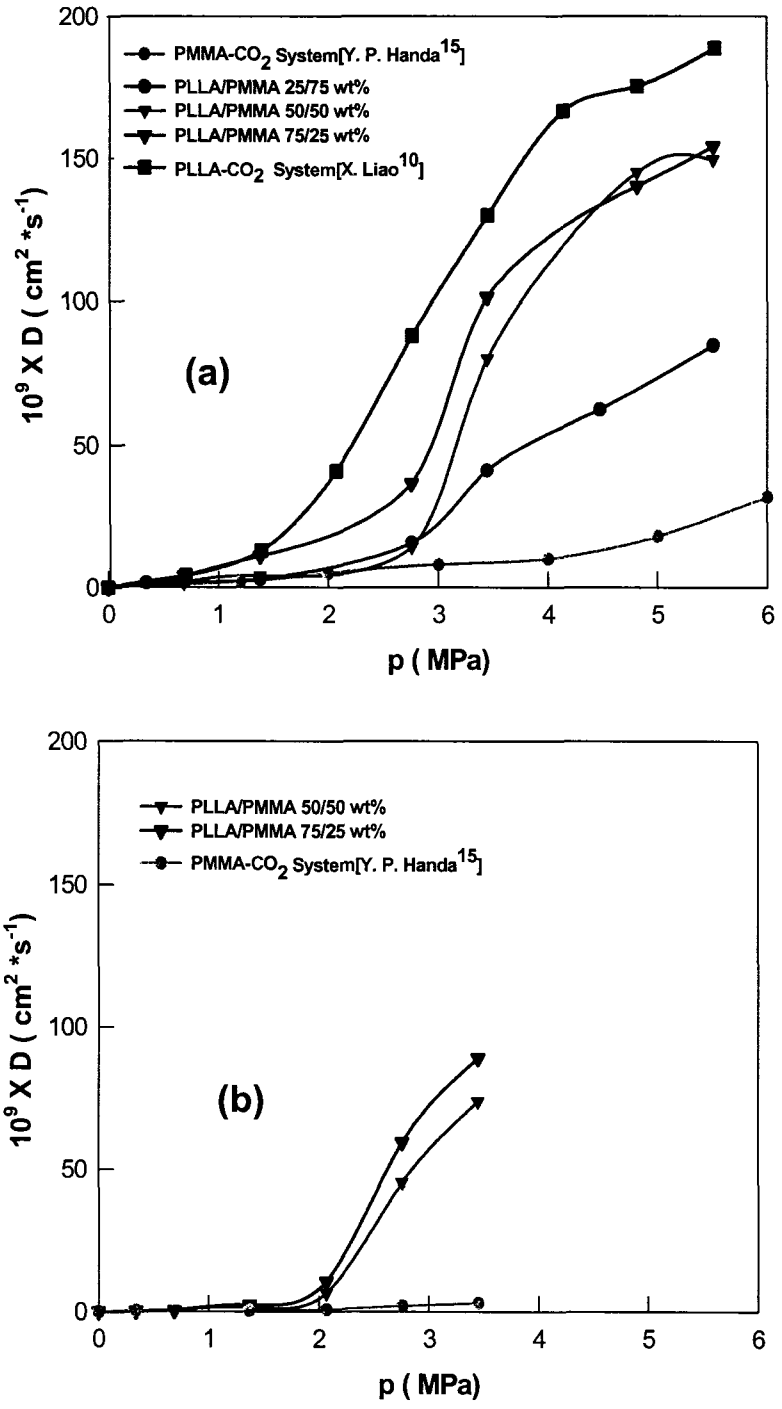

Figure 3.7: Diffusion coefficient of CO_2 in neat and polymer blend samples at: (a) 25°C and (b) 0°C. Curves are drawn through to show trend in data.

Diffusion coefficients of CO_2 in the polymer blend samples as a function of pressure were determined through the sorption kinetic data by means of the hybrid model [13]. The obtained values as compared to those previously reported for PMMA and PLLA–CO_2 systems as well as the solubility data were indicative of the high degree of plasticization in the blends [10-12, 14, 15]. Diffusion coefficients of CO_2 in the blends and neat polymers were found to be concentration dependent and therefore indicating a phase transitions to be occurring in the samples (Figure 3.7).

With a decrease in saturation temperature to 0°C, the solubility of the gas in the polymer increases and the diffusion coefficient increased sharply at lower pressures as compared to the data at 25°C. As previously demonstrated [15]; in the case of PMMA–CO_2 system the higher solubility of the gas results in higher degrees of plasticization and therefore observation of two glass transition temperatures at a constant pressure. Phase transition in polymer-gas systems with favorable interactions is best observed either by high pressure DSC studies or sharp changes in the diffusion coefficient curve as a function of gas pressure [15]. The sudden change in the slope of the diffusion curve has not only been observed in the PMMA–CO_2 system, but also very recently has been observed in the PLLA–CO_2 system [10]. Since the solubility of CO_2 in PLLA/PMMA blend sample is comparable (Figure 3.6); a sudden change in the slope of the diffusion coefficient curve as a function of gas pressure is also observed indicating a phase transition in the system. However; the change in phase from glassy to rubbery state in the case of the PLLA/PMMA blend occurs at a much lower pressure as compared to PMMA (Figure 1.3 of Chapter 1).

Phase transitions in polymer-gas systems can be observed either through experimental data or as previously demonstrated by Condo and Johnston [16] through numerical modeling. Given the results obtained on solubility and diffusion coefficients, PLLA/PMMA-CO_2 system has the potential of exhibiting the retrograde behavior. As such Chapter 4 provides details of the model developed by Condo and Johnston and it application to the system under investigation in the thesis work.

3.3 CO_2 Induced Crystallization

The morphological changes induced by CO_2 were investigated by XRD analysis. The % crystallinity in blends was calculated by comparing the relative area under the crystalline peaks to those obtained from amorphous samples.

Samples as prepared by melt blending and subsequently compression molding and quenching in ice water were amorphous in nature. Figure 3.8 provides the x-ray diffraction pattern for 50/50 wt% PLLA/PMMA sample after being compression molded. As observed, there are no sharp peaks in the diffraction patterns thus indicating the sample to be completely amorphous. This finding also supports the data found in thermal analysis and results obtained in Figure 3.1. Upon contact with CO_2 gas and an increase in pressure the diffraction patterns change and the evolution of a crystalline peak becomes evident (Figure 3.8). The data is very much in support of the solubility data and the formation of a knee in the sorption curves at similar pressure (Figure 3.5).

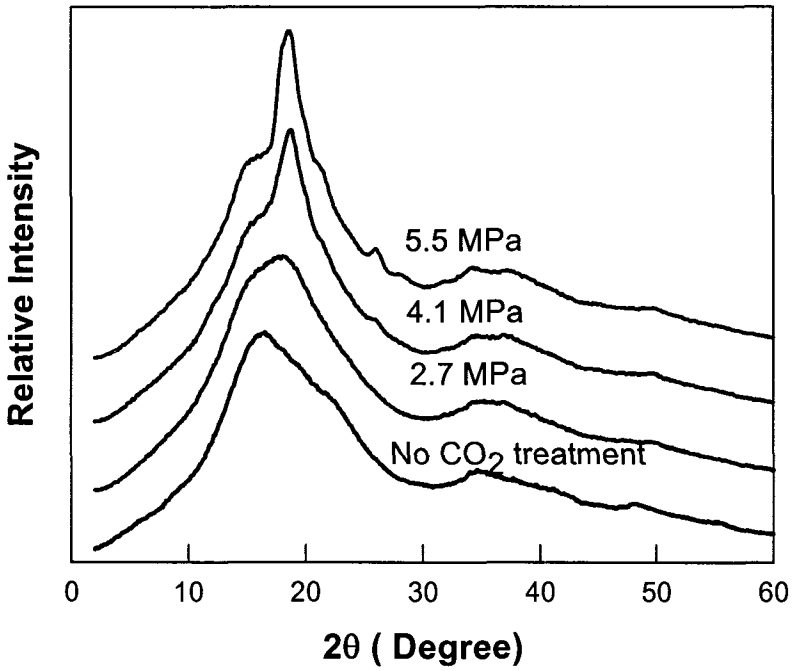

Figure 3.8: X-ray diffraction patterns for PLLA/PMMA 50/50 wt% after exposure to CO_2 as a function of pressures at 25°C.

Similar behavior was also observed for blends with compositions 25/75 and 75/25 wt % after their contact with CO_2. All samples crystallized when treated with CO_2 thus indicating high degrees of relaxation to be occurring in the matrix therefore facilitating the polymer to crystallize (Figure 3.9a). With a decrease in temperature to 0°C the samples are crystallizing however the shape of the peak in the diffraction patterns as observed is somewhat different. The peaks are a little wider indicating the size of the crystals to be smaller (Figure 3.9b).

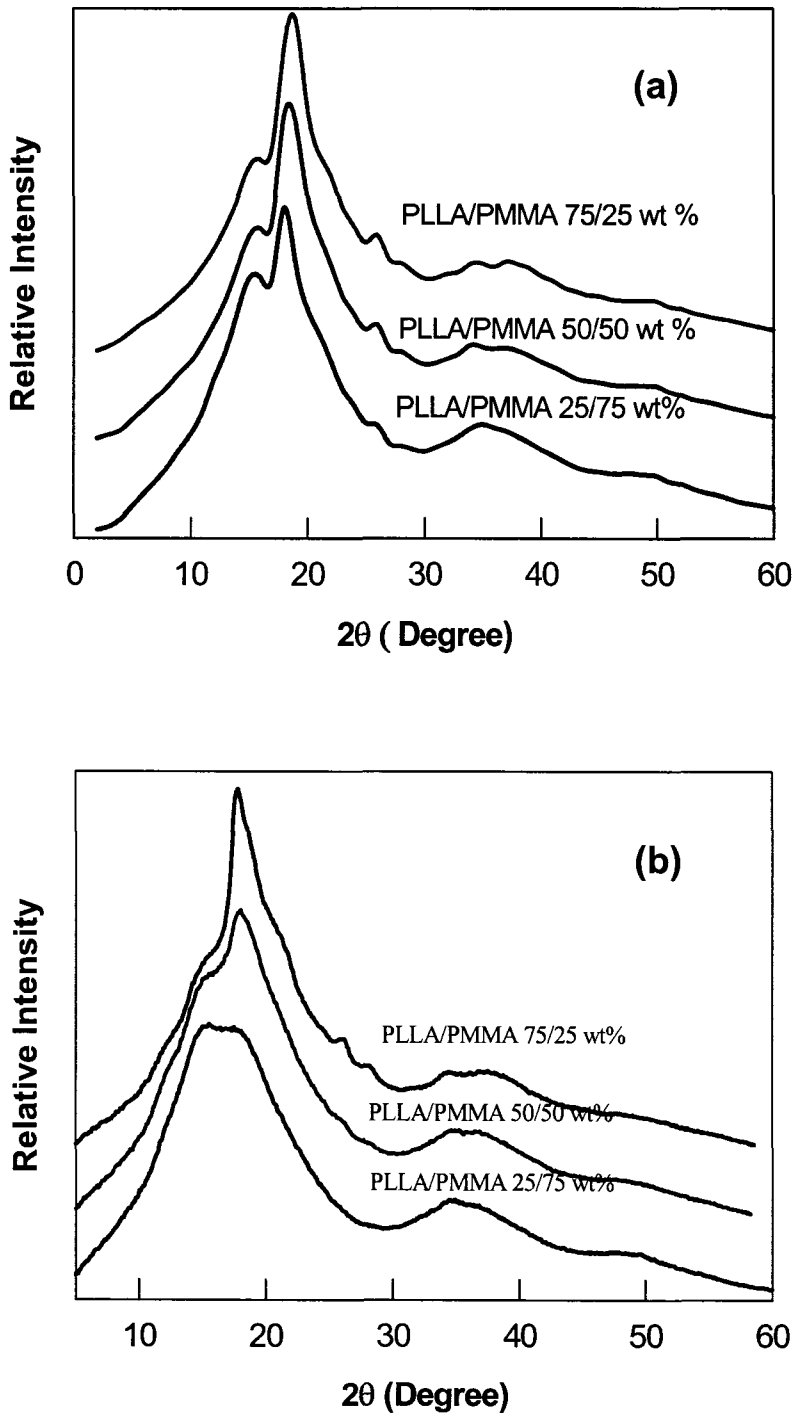

Figure 3.9: X-ray diffraction patterns for the blends as a function of saturation conditions: (a) 5.5MPa CO_2 at 25°C and (b) 3.4MPa CO_2 at 0°C.

The degree of crystallinity in the samples was therefore determined for each sample as a function of pressure (Figure 3.10). Since samples crystallized as a function of saturation pressure a correction to the sorption kinetic data must be applied to reflect on sorption of the gas in the amorphous fraction of the samples. As such, the solubility and diffusivity data were corrected for degree of crystallinity as described in Chapter 1, section 1.5.2. Hence, data presented in Figures 3.6 and 3.7 are for the amorphous fraction of the samples under investigation.

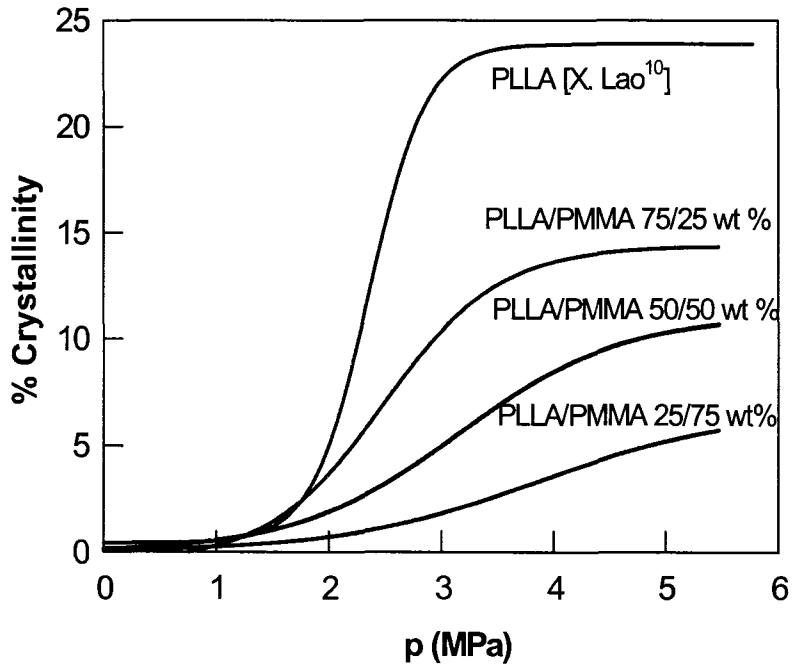

Figure 3.10: Crystallinities of blends after exposed to CO_2 at 25°C.

As observed in Figure 3.10 with the addition of PMMA to PLLA the rate of crystallization is significantly affected. This behavior in samples was also observed in the thermal analysis experiments. Heating polymer samples results in relaxations of the chains and thus facilitating crystallization. Sorption of a gas in a polymer can essentially

do the same through changes in the free volume of the polymer and hence inducing relaxation in the matrix [17]. Either treatment of the samples by heat or CO_2 results in crystallization of the blend matrix and the only factor affecting the rate of crystallization is the content of PMMA in the blends.

3.4 Foam Characterization

The CO_2 blown foams were characterized by foam density, cell density and cell morphologies. The foaming time was set to 30 seconds since no significant difference in foam densities were observed in foams prepared at higher foaming times (Figure 3.11).

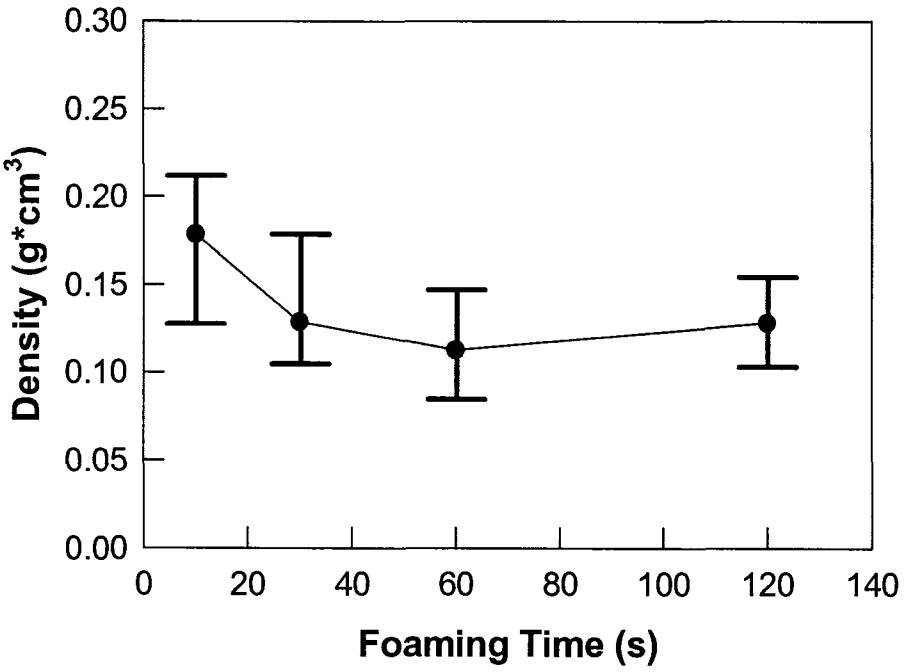

Figure 3.11: The influence of foaming time on foam densities of PLLA/PMMA 25/75 wt%, saturated at 25°C, 5.5MPa and subsequently foamed at 80°C. Curve is drawn through to show trend in data.

Foam densities were strongly dependent on the saturation conditions and foaming temperatures. Higher foaming temperatures resulted in more cells to be nucleate therefore producing foams with lower densities. Furthermore, an increase in the solubility of the gas resulted in more cells to be nucleated thus also affecting the foam densities in the samples. Other factors affecting the foams and morphologies in the samples were the ratio of each component in the blend samples and the results are presented in Figure 3.12. With addition of PMMA to PLLA foam densities as low as 0.1 g / cm^3 were obtained in 25/75 and 50/50 wt% PLLA/PMMA blend samples saturated with 5.5 MPa CO_2 at 25°C and subsequently foamed at 80°C. This yields a substantial reduction in density when compared to a density of 1.2 g / cm^3 for the un-foamed samples (Figure 3.12 a & b). In the case of 75/25 wt% sample a minimum foam density of 0.2 g / cm^3 was obtained at a saturation pressure of 4.1 MPa (Figure 3.12 c). With an increase in saturation pressure an increase in crystallinity was observed thus hindering the nucleation of cells at this foaming condition.

With an increase in foaming temperature past 80°C no significant improvement on the morphologies of the foams in all compositions were observed. In fact foams prepared at 130°C resulted in collapse of the pores and an increase in foam density. In the case of PMMA best foams are obtained as reported in the literature at 90°C at similar saturation conditions. With respect to neat PLLA polymer the best foaming conditions at similar saturation conditions has been observed to be at 80°C. These findings are very much in-line with our finding on the best foaming conditions for the blend samples.

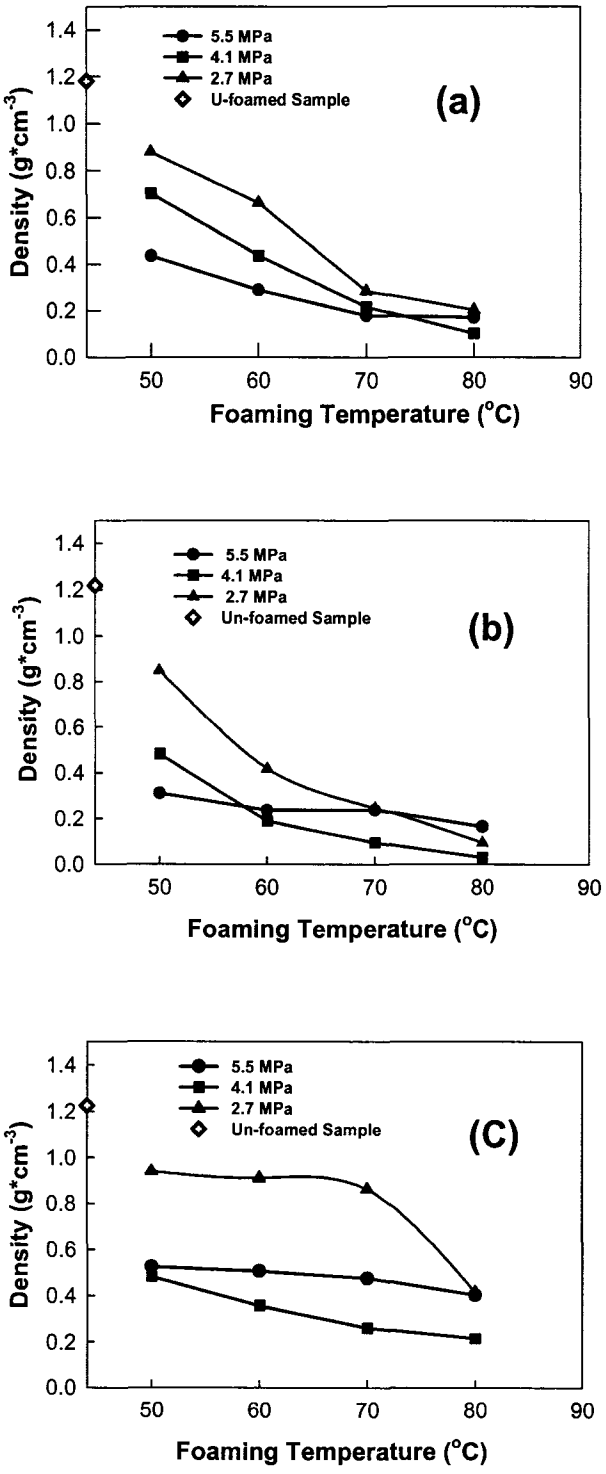

Figure 3.12: Foam densities in the PLLA/PMMA blend samples as a function of foaming temperature, saturation conditions at 25°C; (a) 25/75 wt%, (b) 50/50 wt%, and (c) 75/25 wt%. Curves are drawn through to show trend in data

Formation of crystalline domains in polymers as a result of either heat or CO_2 can have two effects on the foaming process. In some cases it can hinder nucleation and as such it results in higher foam densities. In cases whereby the crystals are small a lower foam density is obtained due to crystals themselves acting as nucleating sites for cell growth. Studies have previously demonstrated that crystalline domains can enhance cell nucleation and therefore result in foams with submicron-cell sizes, higher cell densities and lower foam densities [18, 19]. Our observations on the foaming of PLLA/PMMA samples with higher PLLA content therefore resemble the studies reported in the literature on the positive aspects of crystallinity content on foaming. In certain conditions (saturation and foaming temperatures) the crystals are small enough to have a positive effect thus resulting in lower foam densities (Figure 3.12 c).

With a decrease in saturation temperature a much milder pressure was needed to reach similar solubility in the samples as compared to samples saturated at 25°C. This therefore also affected the foaming of the samples when saturated with CO_2 at 0°C and 3.4MPa. Foam densities are similar to those obtained when saturated at 25°C, however, the rate of cell nucleation as a function of foaming temperature is much faster for samples saturated at 0°C than those reported at 25°C (Figure 3.13, Figure 3.15). Foam densities as low as 0.3 g / cm^3 were obtained when samples were foamed at 80°C. With an increase in temperature no further reduction in density was observed.

The cell densities for foamed blends are given in Figure 3.14 and Figure 3.15; as observed foaming temperature and saturation pressure affects cell density significantly.

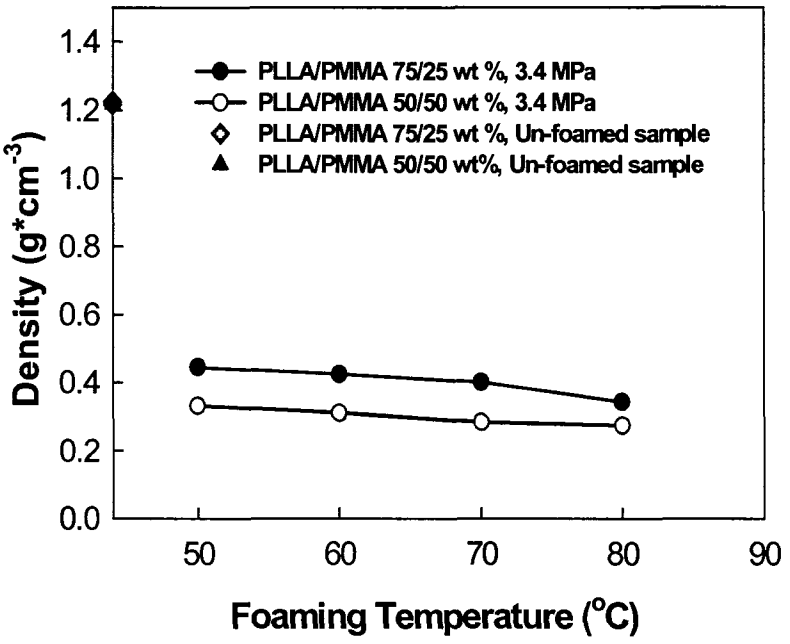

Figure 3.13: Foam densities in the blend samples as a function of foaming temperature, saturation conditions of 3.4 MPa and 0°C. Curves are drawn through to show trend in data

In the 25/75 and 50/50 wt% samples with an increase in saturation pressure a higher cell density is obtained in the foamed samples at 80°C. With an increase in the foaming temperature no further improvement in the cell densities were observed. However; in the 75/25 wt% samples even though an increase in the saturation pressure to 5.5 MPa did not improve on the foam densities due to formation of crystalline domains, an improvement on the cell density is observed. The measurement of foam densities provides information on the bulk properties of the sample. Cell densities however provide information on the amorphous fraction of the sample as they are foamed. Therefore, with an increase in pressure a higher cell density at 80°C in this sample is obtained.

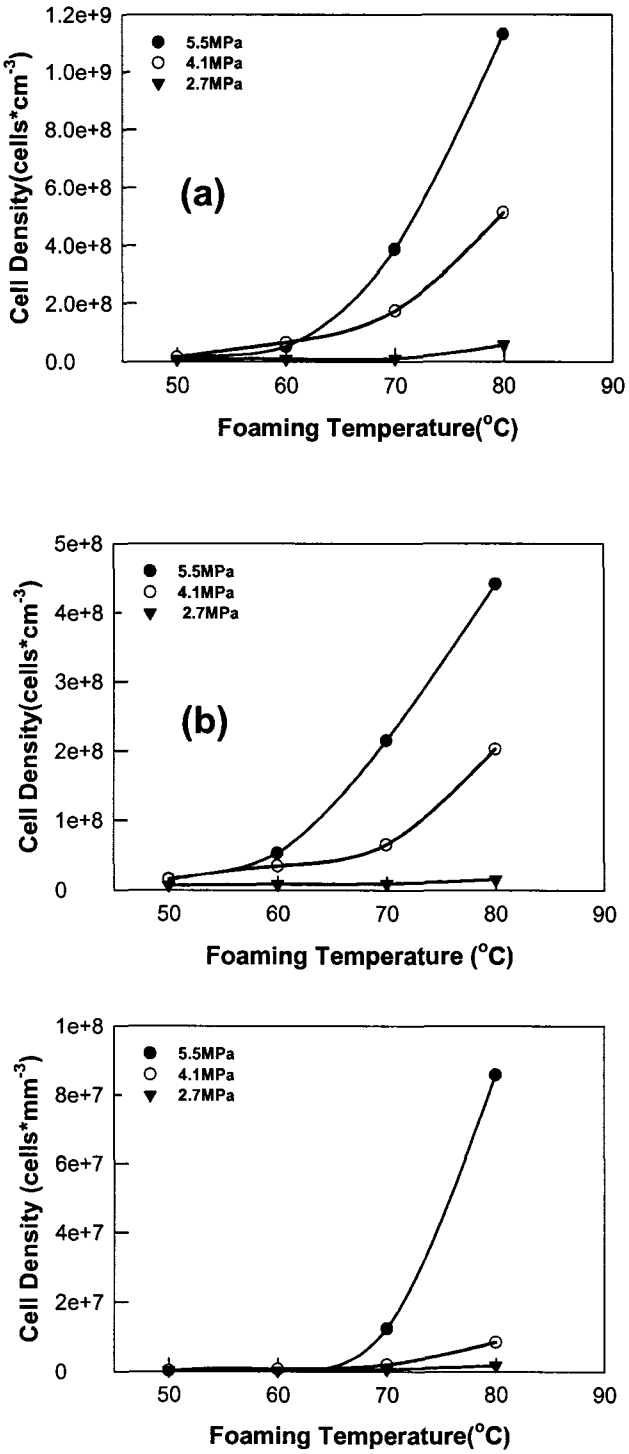

Figure 3.14: The influence of foaming temperature on cell density as a function of pressure at 25°C: (a) 25/75, (b) 50/50 wt% and (c) 75/25 wt%. Curves are drawn through to show trend in data

The effect of a decrease in the saturation temperature on cell density of foams is

presented in Figure 3.15. Since no changes in the amount of gas uptake was observed in the samples the cell densities as expected follow the same trend in data as Figures 3.14 b and c.

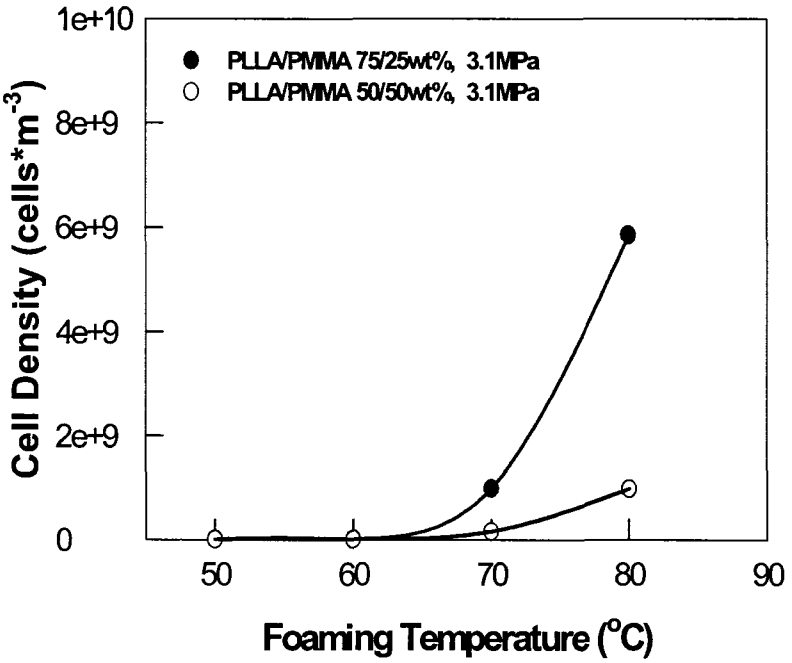

Figure 3.15: The influence of foaming temperature on cell density at a saturation condition of 3.4 MPa, and 0°C. Curves are drawn through to show trend in data

Cell sizes in the foamed samples were determined by analyzing the morphologies using SEM microphotographs. Tables 3.3 and 3.4 provide information on foam cell sizes as a function of saturation conditions and foaming temperatures. At a saturation condition of 5.5 MPa and 25°C the lowest cell size obtained is 3.5 μm in the 50/50 wt% blend sample. With a decrease in saturation temperature and hence a much larger temperature gap more cells are nucleated and as such a much lower cell size is obtained. The lowest cell size was found to be 1.5 μm for the 75/25 wt% samples saturated at 3.4

MPa, 0°C, and subsequently foamed at 70°C. A decrease in the saturation conditions has been found to also affect the cell size in the 50/50 wt% samples. Given the similar equilibrium solubilities in the samples regardless of saturation conditions and foaming temperatures; the large change in cell size therefore can be attributed to a much more effective sudden thermodynamic change in the system.

Table 3.4: Foam average cell size as a function of foaming temperature, saturation conditions of 25°C and 5.5 MPa.

Foaming Temperature(°C)	Average Cell Size(μ m) (25/75 wt%)	Average Cell Size(μ m) (50/50 wt%)	Average Cell Size(μm) (75/25 wt%)
50	19.6	11.2	8.4
60	13.5	9.5	7.5
70	7.8	7.6	4.2
80	5.8	3.5	4.0

Table 3.5: Foam average cell size as a function of foaming temperature, saturation conditions of 0°C and 3.4 MPa.

Foaming Temperature(°C)	Average Cell Size(μ m) (50/50 wt%)	Average Cell Size(μm) (75/25 wt%)
70	3.6	2.5
80	1.8	1.5

Furthermore; higher PLLA content in blends additionally affects cell density due to a lower T_g and a higher free volume available in the samples. This combined with the induced crystallization effects of CO_2 on the samples collectively affects the foam morphologies and cell sizes in the samples.

3.4.1 Foam Morphologies

Foam morphologies of the blends as compared to neat polymers were investigated with respect to effect of pressure and temperature. In the case of PMMA, an increase in gas pressure resulted in an improved foam morphology. A decrease in saturation temperature further affected the morphology of this polymer and resulted in more cells nucleated and thus a more uniform structure to be obtained [15]. In the case of PLLA, an increase in CO_2 pressure attributes to a higher degree of crystallinity, thus affecting the cellular structure dramatically [10]. Figure 3.16 provides SEM microphotographs of PLLA/PMMA 50/50 wt % foamed at 70°C with CO_2 at a saturation condition of 4.1 MPa and 25°C. The structures obtained for the neat polymers are not fully expanded (PMMA), and regionally foamed (PLLA). The foam structure for the blend is however somewhat uniform indicating a slight improvement over neat PLLA. With an increase in pressure and foaming temperature combined with changes in the blend compositions dramatic changes in the morphologies were observed. Though both polymers are FDA approved, most foam morphologies obtained at the above saturation conditions of 25°C were closed cell foams. The obtained morphologies remain to very useful in many industrial applications provided the materials meet specifications on mechanical properties. For example blending a petrochemical base resin with a biopolymer can provide a more viable way to producing materials that are more environmentally acceptable. Given the morphological modifications and improvements observed for neat PLLA polymer, a number of foaming parameters (T and p changes) were investigated and samples were analyzed by SEM microphotographs.

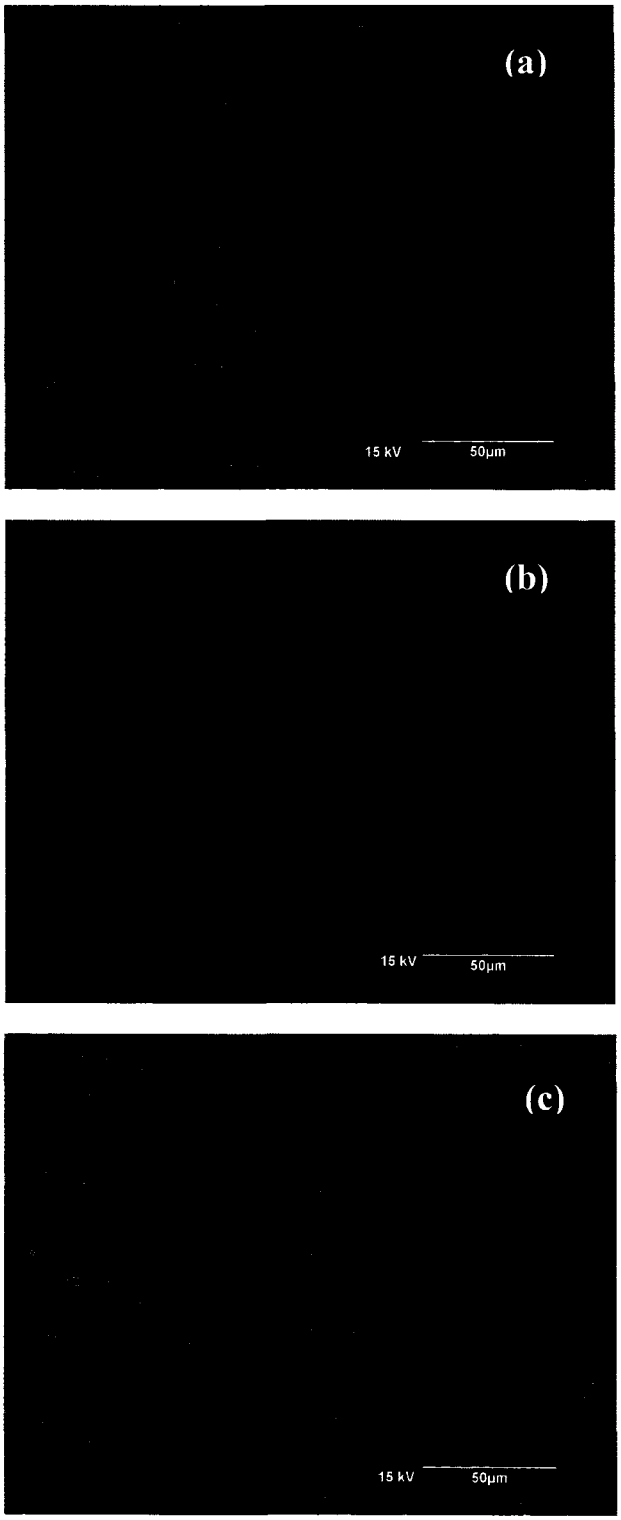

Figure 3.16: SEM microphotographs of polymer samples foamed at 70°C, CO_2 saturation condition of 4.1MPa and 25°C: (a) PLLA/PMMA 50/50wt%, (b) PMMA and (c) PLLA.

With an increase in saturation pressure to 5.5 MPa as observed in Figure 3.17 an improvement on the morphologies of the blends is observed when foamed at 80°C. Figure 3.17a represents foams in a 25/75 wt% PLLA/PMMA blend sample. The morphology is not uniform and the cell sizes range from small to large with regions exhibiting foam collapse. With an increase in PLLA composition to 50% significant improvement on the morphology is observed due to creation of higher free volume in the sample and changes with respect to crystallization of the polymer (Figure 3.17 b).

Foams with higher PLLA content resulted in a unique structure even though at times not very uniform (Figure 3.17 c). A closer look at the structures in the 75/25 wt% PLLA/PMMA samples indicated the possibility of generating an interconnected and porous structure. In this particular blend compositions foamed at 80°C cell walls have become much thinner and some neighboring cells could be clearly noted on the SEMs. However; with an increase in foaming temperature no significant improvement on the porous structure was observed. Creating an open and interconnected porous structure with CO_2 requires a very specific processing condition. Therefore; batch studies as conducted in this research work can serve as a very useful tool on finding such processing window.

Pore nucleation and growth is related to the solubility and diffusion behavior of CO_2 as well as the rheological properties of the polymer. Physical property changes of the blends induced by CO_2 play an important role on the sorption behavior of gases, and therefore affect cell nucleation and growth rates in such matrices. A change in saturation condition was therefore studied on its effect on formation of porous morphologies in a

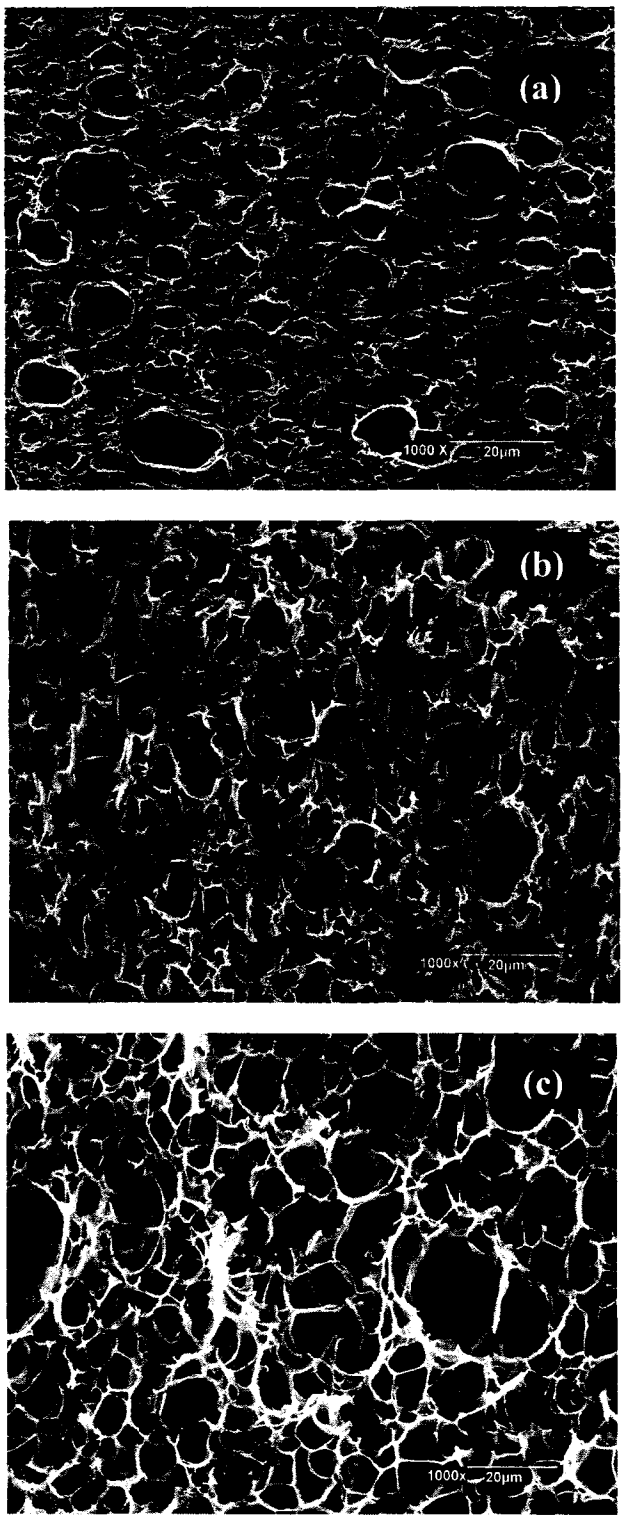

Figure 3.17: SEM microphotographs of PLLA/PMMA saturated with CO_2 at 5.5 MPa, 25°C, and foamed at 80°C: (a) 25/75, (b) 50/50, and (c) 75/25 wt% samples.

50/50 and 75/25 wt% samples as both exhibited unique morphologies when treated with CO_2.

Morphologies of foams with composition 50/50 wt%, 75/25wt % as prepared at saturation at 0°C and 3.4 MPa are presented. Due to a larger temperature gap between saturation and foaming, the created foams had higher cell density and small cell size (Figure 3.18). The obtained foams have partly microcellular and open cell structure.

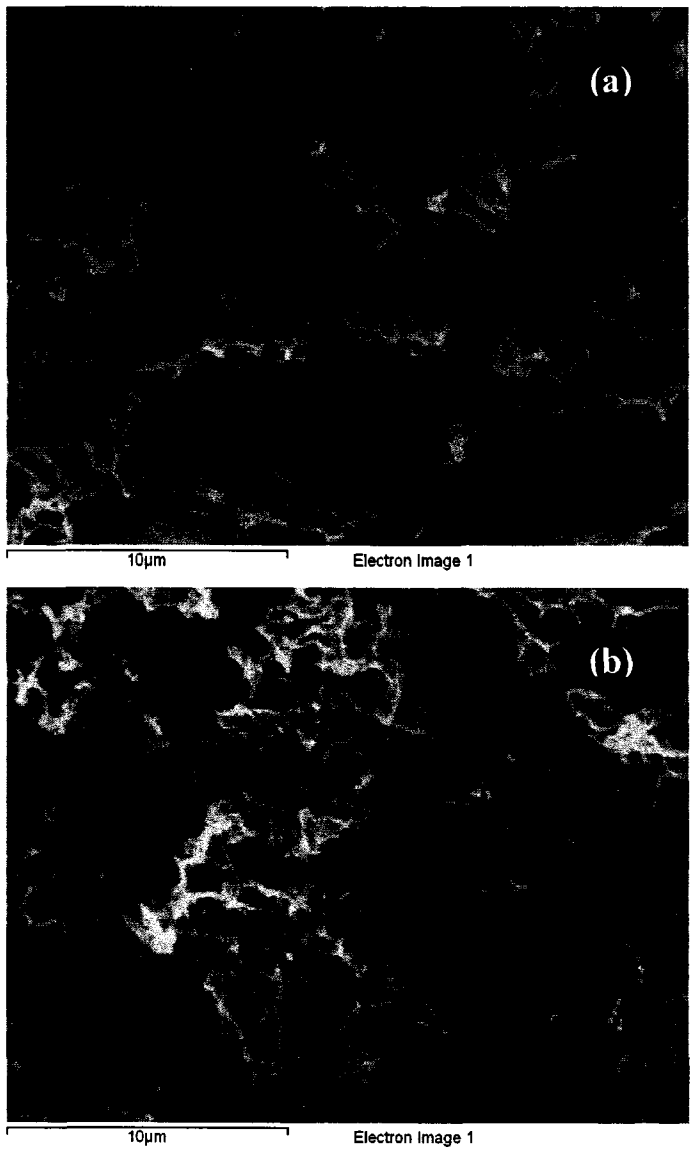

Figure 3.18: SEM microphotographs PLLA/PMMA samples saturated with CO_2 at 3.4MPa and 0°C and subsequently foamed at 80°C (a) 50/50, (b) 75/25 wt%.

The samples prepared at a saturation condition of 3.4 MPa, and 0°C exhibit very unique morphological characteristics. A closer look at the foams in Figure 3.18 indicates some degree of openness and interconnections in the samples between the cells. Such structures have a great deal of potential applications in the biomedical industry as scaffolds for tissue engineering applications. Since both PLLA and PMMA are FDA approved, the above generated structures can then be used as a growth medium for tissue with no danger to the surrounding organs. Furthermore, the process by which the matrices have been generated is solvent free and thus no residual solvents are present to pose harm towards the transplanted cells.

A further step in this research process can in fact be the seeding of the structures as presented in Figure3.18 and observing tissue growth.

References

1. Zawada, J.A.; Ylitalo, C.M.; Fuller, G.G.; Colby, R.H.; Long, T.E. *Macromolecules* **1992**, 25, 2896-2904.

2. Pathak, J.A.; Colby, R.H.; Floudas, G.; Jerome, R. *Macromolecules* **1999**, 32, 2553-2559.

3. Liao, X.; Nawaby, A. V. ; Handa, Y. P. *Cellular Polymer* **2007**, 26, 69-81.

4. Zhang,G.; Zhang, J.; Wang, S.; Shen, D. *Journal of Polymer Science: Part B: Polymer Physics* **2003**, 41, 23-30.

5. Errco, M. E. *Current Trends in Polymer Science* **1999**, 4, 1-26.

6. Le, K. P.; Lehman, R. ; Pemmert, J. ; Vanness, K. ; Ward, P. M. L.; Idol, J. D. J. *Biomater. Sci. Polymer Edn.* **2006**, 17, 121-137.

7. Ohkoshi, I., Abe; H.; Doi, Y. *Polymer* **2000**, 41, 5985-5992.

8. Marquez, L.; Sabino, M.A.; Rivero, I.A. *Polymer Bulletin* **1998**, 41, 191-199.

9. Knapp, A. M.; Halloran, J. W. *J. Am. Ceram. Soc.* **2006**, 89, 2776-2785.

10. Liao, X.; Nawaby, A. V.; Day, M. Layered Open Cell Poly ($_L$-lactic acid) Nanomorphology, *ACS* **2005**, Washington, USA.

11. Baldwin, D. F.; Shimbo, M.; Suh, N. P. *Journal of Engineering Materials and Technology* **1995**, 117, 62-70.

12. Sato, Y.; Yamane, M.; Sorakubo, A.; Takishima, S.; Masuoka, H.; Yamamoto, H.; Takasugi, M. *The 21st Japan Symposium on Thermophsical Properties* **2000**, Nagoya, Japan, 196-203.

13 . Wong, B.; Zhang, Z.; Handa,Y. P. *Journal of Polymer Science: Pare B: Polymer Physic* **1998**, 36, 2025-2032.

14. Manninen, A. R.; Naguib, H. E.; Nawaby, A.V.; Day, M. *Polymer Engineering and Science* **2005**, 45, 904-1001.

15. Handa, Y. P.; Zhang, Z.; Wong, B. *Cellular Polymer* **2001**, 20, 1-16.

16. Condo, P.D.; Sanchez, I. C.; Panayiotou, C.G.; Johnston, K.P. *Macromolecules* **1992**, 25, 6119-6127.

17 . Chiou, J. S.; Barlow, J. W. and Paul , D. R. *Journal of Applied Polymer Science* **1985**, 30, 3911-3922.

18. Han, X. H.; Lee, L. J.; Tomasko, D.L. *Aust. J. Chem.* **2005**, 58, 492-450.

19. Itoh, M.; Kabumoto, A. *Furukawa Review* **2005**, 28, 32-40.

Chapter 4

Prediction of Gas Solubility, Polymer Swelling and Glass Transition Behaviors in PLLA/PMMA-CO_2 System

4.1 Introduction

Gas solubility in a polymer can be determined by a gravimetric method, however in some cases it can be time consuming [1, 2]. The glass transition temperature in polymer-gas systems can be determined experimentally through high pressure DSC measurements, however the steps are lengthy and the data analyses are somewhat tedious.

The dual-mode sorption model has been used successfully to describe the convex shape of solubility in glassy polymers. The three parameters in this model; Langmuir adsorption parameter, Langmuir affinity parameter and Henry's law solubility coefficient (Chapter 1, equation 1.7) can be found by fitting the model to the experimental data [3, 4]. This model is simple and can only be used in a limited temperature and pressure range where the regression is performed. Furthermore; this model can not interpret some physical changes of the polymer-gas system during sorption such as polymer dilation.

In the last decade many alternative models have been developed to describe gas solubility in glassy polymers. The Sanchez-Lacombe equation of state (S-L EOS) is often used to describe polymer-gas systems because of its inherent ability to handle correlating multiple thermodynamic properties in these systems. A combination of S-L EOS, solution equilibrium theory, and Gibbs-Dimarzio dynamic criterion for glass transition can aid in predicting many thermodynamic properties of a polymer-gas system [5-10].

The use of S-L EOS to calculate the solubility of a gas in a polymer blends can be a challenging work since the P-V-T data for blends is related to the composition and the interaction parameters of the gas and two polymers. Though characteristic parameters are available for most neat polymers (including PMMA and PLLA), characteristic parameters of blends change with blend composition. To the best of our knowledge, the characteristic parameters of PLLA/PMMA and binary interaction parameter of PLLA/PMMA-CO_2 are not available in the literature.

In this study, the interaction parameters of CO_2 with PLLA/PMMA were calculated by best fitting the S-L EOS to experimental solubility data. Moreover, the solubility of CO_2 in PLLA/PMMA blends was predicted for variable system pressures at 25°C using obtained interaction parameters. This system temperature was used since data and parameters were available in the literature. The increase in intramolecular energy for blends due to flexing of a bond was calculated using glass transition data in ambient condition. The glass transition behaviors of PLLA/PMMA-CO_2 system in various compositions were predicted using obtained interaction parameters of CO_2 with PLLA/PMMA and increased intramolecular energy using S-L EOS, solution equilibrium theory and Gibbs-Dimarzio dynamic criterion for glass transition. The models to be used and described in this section are well established and published. Furthermore, the models have been used previously on PMMA-CO2 system [6, 9].

4.2 Theory

S-L EOS equation, theories of solution equilibrium and Gibbs-Dimarzio dynamic criterion for glass transition were basic theories to predict gas solubility and glass

transition behaviors in a polymer-gas system, which were given in Chapter 1, section 1.5.1.

In this study, there are two binary system, polymer-polymer binary system and gas-blend system. In order to use S-L EOS for blend-CO_2 system, the characteristic parameters of blends must be first known. For a polymer-polymer system, the characteristic parameters of blend change with the composition and are related to the binary interaction energy between two polymers. In this study, characteristic parameters of blends were calculated based on following equations 4.1 through 4.6 [11, 12]:

$$\phi_i = \frac{m_i / \rho_i^*}{[m_1 / \rho_1^* + m_2 / \rho_2^*]} \quad \textit{for i=1 and 2} \tag{4.1}$$

$$\phi_i^0 = \frac{\phi_i}{\phi_1 + (\upsilon_1^* / \upsilon_2^*)\phi_2} \quad \textit{for i=1 and 2} \tag{4.2}$$

$$1/\rho^* = m_1/\rho_1^* + m_2/\rho_2^* \tag{4.3}$$

$$\upsilon^* = \phi_1^0 \upsilon_1^* + \phi_2^0 \upsilon_2^* \tag{4.4}$$

$$P^* = \phi_1 P_1^* + \phi_2 P_2^* - \phi_1 \phi_2 \Delta P^* \tag{4.5}$$

$$T^* = P^* V^* / R \tag{4.6}$$

where, m_i, ϕ_i and ϕ_i^0 are weight fraction, closed packed volume fraction and mole fraction of component i in the mixture, respectively; ρ^*, P^* and T^* are characteristic parameters; R is gas constant; and ΔP^* is the actual energetic interaction (binary interaction energy) between components [13]. Binary interaction energy of crystalline

polymer - amorphous polymer can be calculated based on available melting depression [14, 15]. The interaction energy is small and value of ΔP^* can be ignored for calculation of P^*. So, equation 4.5 is approximately expressed by:

$$P^* = \phi_1 P_1^* + \phi_2 P_2^* \tag{4.7}$$

For a binary system consisting of blend-CO_2 system, the binary interaction parameter (ς_{12}) is calculated by fitting experimental solubility data to S-L EOS (equation 1.10), and conditions of equilibrium (equation 1.26 and 1.27).

In order to calculate the glass transition temperature in polymer-gas systems, Gibbs-Dimarzio dynamic criterion for glass transition is also needed. In Gibbs-Di Marzio dynamic criterion, the entropy (S) of polymer-gas system is equal to zero in glass transition state. In the glass transition conditions, polymer-gas system is also satisfying S-L EOS (equation 1.10), and conditions of equilibrium (equation 1.26 and 1.27).

For using Gibbs-Dimarzio dynamic criterion for glass transition (equation 1.31, 1.32), the increase in intramolecular energy due to the flexing of a bond was calculated using T_g obtained under ambient condition (0.1013MPa air and 25°C). It was assumed that there was no CO_2 dissolved in the blends under ambient condition and the increase of intramolecular energy did not change with system's CO_2 pressure. Coordination number of the lattice was chosen as 5 or 10 based on recommendations by Condo [6, 16] on studies performed on PMMA-CO_2 system.

4.3 Results and Discussion

4.3.1 Characteristic Parameters of PLLA/PMMA Blend System and Interaction Parameters of PLLA/PMMA-CO_2 System

The equilibrium solubility data of CO_2 in PLLA/PMMA blends at room temperature were collected by in-situ gravimetic analysis in this research work. Weight fraction of CO_2 in polymers can be calculated using equations 2.6, 2.7 and 1.35. The characteristic parameters for blends were calculated using equation 4.1-4.7 and the data is given in Table 4.1. The binary interaction parameters were calculated by fitting experimental solubility data to S-L EOS (equation 1.10), and condition of equilibrium (equation 1.26 and 1.27)

Table 4.1: Characteristic parameters and interaction parameters at 25°C.

Substance	P* (MPa)	T* (K)	ρ *(kg*cm^{-3})	M_w	ς_{12}
CO_2 [6]	574.0	308.6	1505	44.01	
PLLA [17, 18]	559.2	631.0	1333	63370	1.141
PMMA [1, 6]	503.0	696.0	1269	10850	1.153
PLLA/PMMA 25/75 wt%	523.1	668.9	1284	97220	1.138
PLLA/PMMA 50/50 wt%	538.2	651.6	1300	85930	1.131
PLLA/PMMA 75/25 wt%	549.9	639.7	1316	74650	1.137

a- actual molecular weight

The temperature dependent of the binary interaction parameter for PLLA/PMMA-CO_2 system is also related to the composition of the blends. The relationship is presented in Figure 4.1.

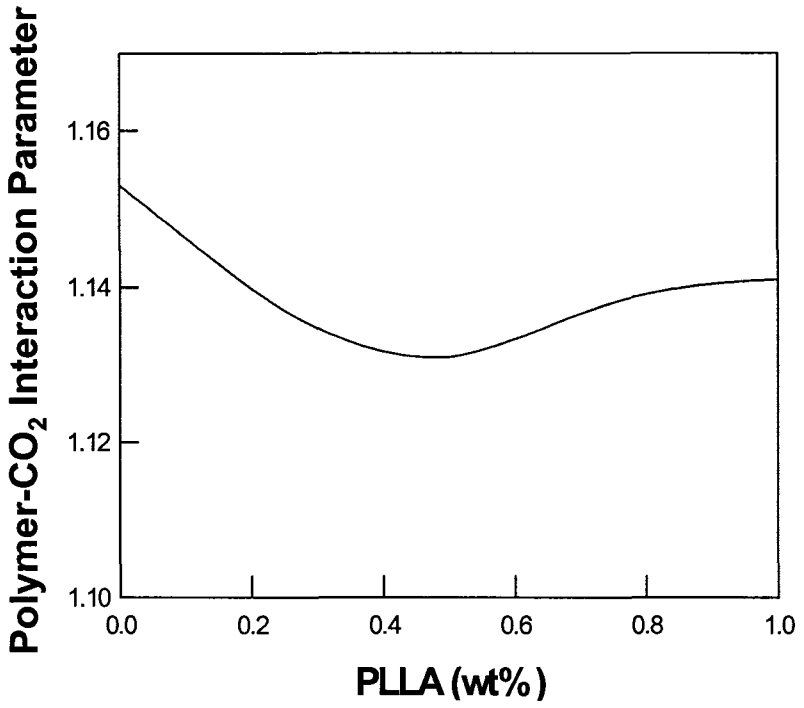

Figure 4.1: Interaction parameters as a function of PLLA composition in the blend at 25°C.

Gas solubility is strongly affected by the interaction parameter and related to the polymer characteristic parameters. Compared to pure PMMA-CO_2 and PLLA-CO_2 systems, the interaction parameter for PLLA/PMMA-CO_2 is lower than either one. Therefore; the interaction of polymer-CO_2 was weakened by blending and even the possibility of existence of an interaction between PLLA and PMMA polymers themselves.

4.3.2 Prediction of CO_2 Equilibrium Solubility in PLLA/PMMA

The solubility of CO_2 in PLLA/PMMA blends at a wide pressure range was predicted based on the obtained blend-CO_2 interaction parameters, results are presented in Figure 4.2.

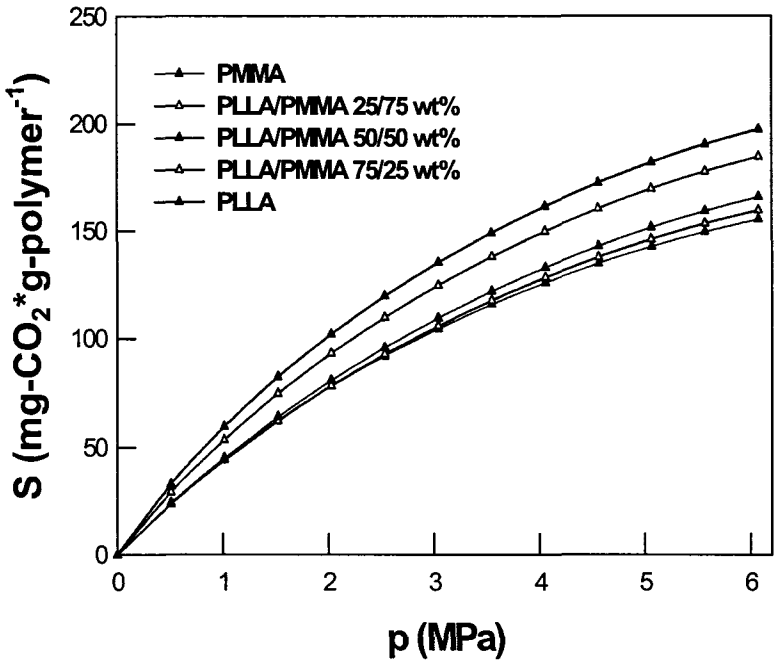

Figure 4.2: Predicted solubility of CO_2 in blends and neat polymers at 25°C.

Figure 4.3 provides a comparison between the predicted solubility data to those obtained through experiments for the blend-CO_2 system at 25°C. There are two reasons for the mismatch between predicted solubility and experimental solubility.

The influence of volumetric expansion caused by CO_2 sorption is negligible for low pressures, however; it has a much stronger effect at higher pressures. For PLLA/PMMA blends, the glass transition as observed through experimental data takes place at much lower pressures at room temperature and as such the volumetric expansion should be taken into account in the in-situ gravimetric solubility measurement. In another words, the experimental solubility data should be corrected by the swelling factors.

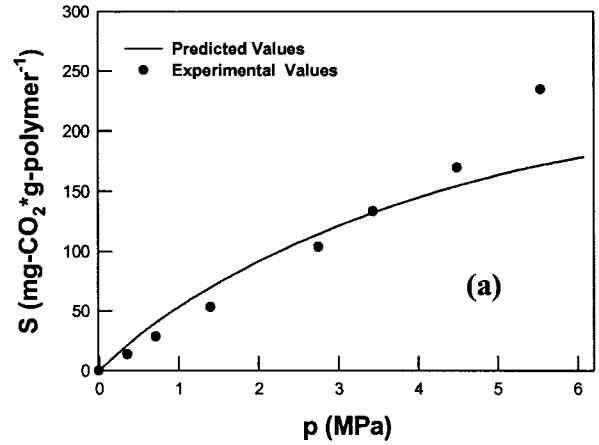

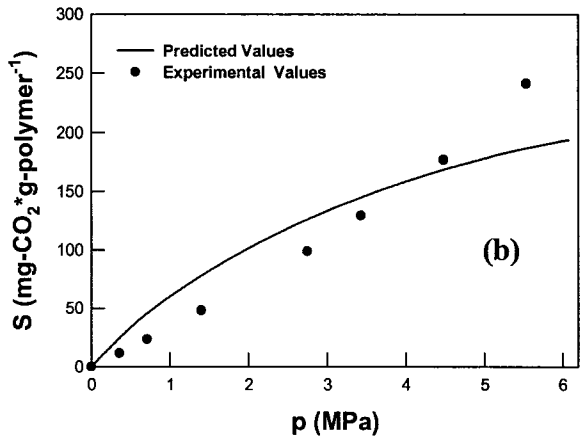

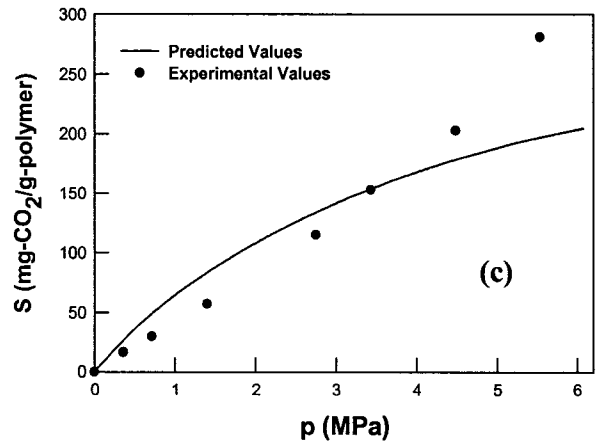

Figure 4.3: Predicted solubility and experimental solubility at 25°C, (a) 25/75 (b) 50/50, and (c) 75/25 wt% PLLA/PMMA samples.

Another reason for the mismatch is that S-L EOS is based on the model of a molecular fluid, in which all mers are in a thermodynamic equilibrium. Therefore; for polymer-gas systems, the regular S-L-EOS is not valid to describe the system when the polymer is in the glassy state [9]. In this study the system undergoes a transition and as such some solubility data is obtained in the glassy state and some in the rubbery state.

4.3.3 Prediction of Solution Equilibrium Swelling

In a lattice fluid model, the fraction of occupied sites (or reduced density $\overline{\rho}$) is defined by:

$$\overline{\rho} = \frac{rN}{N_0 + rN} \tag{4.8}$$

$$\gamma = \mathrm{P}^* \upsilon^* / (R\,T^*) \tag{4.9}$$

Where; N_0 and rN are vacancy lattices and lattices occupied by the components respectively. P^*, υ^* and T^* are characteristic parameters for the binary system. The swelling factor (S_w) is defined as [9]:

$$S_w = V_{mix} / V_0 \tag{4.10}$$

Where V_{max} and V_0 represent the volume of mixture and neat polymer. In this study, it was assumed that polymer swelling is only caused by an increase in the vacant sites as created by gas dissolving in the matrix. Therefore, the swelling factor is given by:

$$\mathrm{S_w} = (\overline{\rho}\ )_{\mathrm{p=0}} / (\overline{\rho}\ )_{\mathrm{p}} \tag{4.11}$$

($\bar{\rho}$)$_{p=0}$ and ($\bar{\rho}$)$_p$ are the reduced density of the mixture at systems$_2$ pressure p and 0 respectively.

Swelling factors for PLLA/PMMA blends and neat polymers are calculated by combining S-L EOS and equation $\mu_1^0 = \mu_1$, the results of which are presented in Figure 4.4.

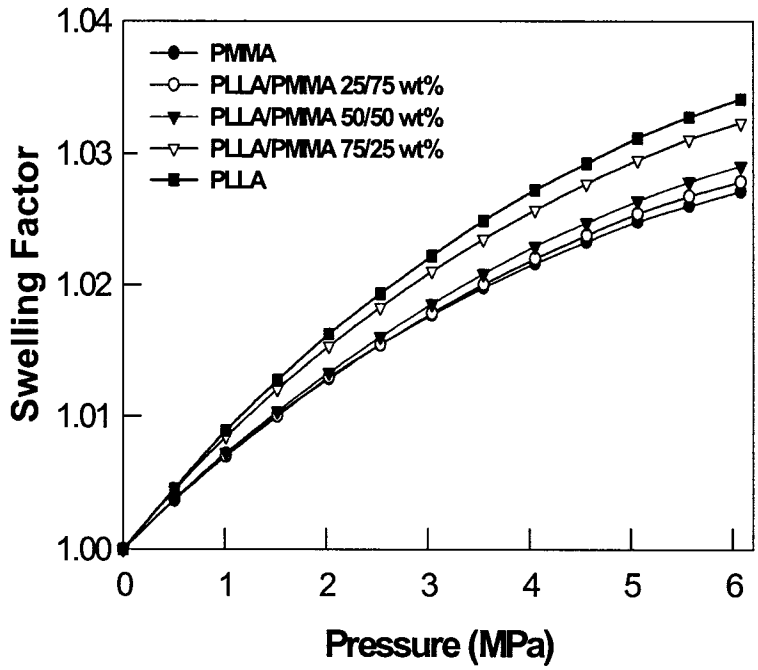

Figure 4.4: Equilibrium swelling of PLLA/PMMA blends and neat polymers at 25°C.

When the system's pressure is increased, more CO_2 becomes dissolved in the blends and as such more vacancies are created in the matrix. A plot of swelling factor versus pressure was similar to the plot of solubility for PLLA/PMMA blends at the same conditions.

The predicted swelling data are useful for correcting the experimental solubility data. The interaction parameter for blend-CO_2 can then be recalculated based on corrected solubility data. Through iteration, the best match between experimental solubility data and predicted solubility data can be found in future studies in this area.

4.3.4 Prediction of Glass Transition Behaviors in PLLA/PMMA

In the polymer-gas systems dissolution of gas increases the free volume, enhances polymer chain mobility and lowers the glass transition temperature [9]. So, the T_g is related to the system's pressure.

Table 4.2: Flex energy of blends and neat polymers.

Substance	T_g(°C)	$\Delta\varepsilon_i$ (J/mol, Z=10)	$\Delta\varepsilon_i$ (J/mol, Z=5)
PLLA	54.1	10112	6336
PMMA	106.7	11854	7443
PLLA/PMMA 25/75wt%	85.1	11126	7076
PLLA/PMMA 50/50wt%	66.6	10953	6764
PLLA/PMMA 75/25wt%	58.9	10595	6525

From Gibbs-Di Marzio dynamic criterion for glass transition (Equation 1.31 and 1.32), the entropy of mixture is related to the lattice coordination number (Z) and the increase of intramolecular energy ($\Delta\varepsilon_i$) due to the flexing of a bond in a type i chain

molecule. The values of $\Delta\varepsilon_i$ were deduced from equation 1.31 using known glass transition temperatures under ambient conditions. The values are strongly dependent on the lattice coordination number (Z) and are given in table 4.2.

The glass transition behaviors of PLLA/PMMA-CO_2 system were predicted in this study using the obtained interaction and characteristic parameters for the system. The predicted T_g is presented in Figure 4.5.

There are two regions in Figure 4.5 and 4.6 inside the P-T_g curve which presents the physical state of the polymer in contact with the gas. This information is rather an important one simply because foams prepared from the glass state are very different than when prepared from the rubbery state. Blends, neat PLLA and PMMA all exhibit retrograde vitrification. The experimental results of T_g for PMMA-CO_2 system presented by Honda [19] is a perfect example of a match between predicted results and experimental data for this system. The Tg of PLLA, PLLA/PMMA blends are much lower than PMMA and not far from the critical temperature of CO_2 (31.1°C). The solubility of CO_2 in PLLA and its blends is somewhat large at lower temperature and change rapidly with temperature. So, the retrograde transition from glassy to rubbery state is possible and some evidence of it was observed from the experimentally obtained diffusion coefficients [20]. Using the appropriate parameter we have thus demonstrated the possibility of this behavior using the established model and have used it to generate intriguing morphologies from the PLLA/PMMA system via processing with CO_2.

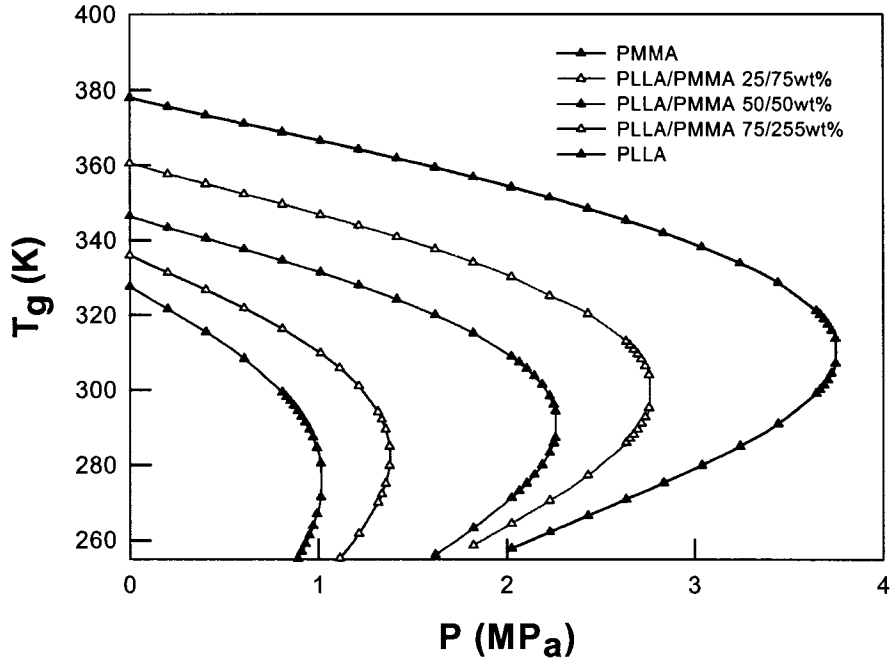

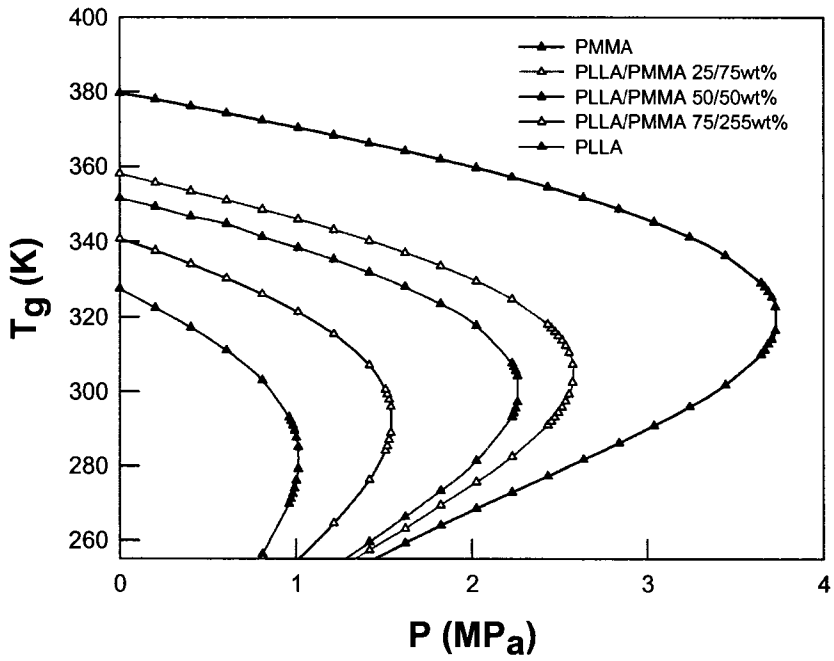

Figure 4.5: Predicted T_g as a function of system pressure at 25°C: (a) Z=5, (b) Z=10.

References

1. Handa, Y. P.; Zhang, Z.; Wong, B. *Cellular Polymer* **2001**, 20, 1-16.

2 . Wong, B.; Zhang, Z.; Handa, Y. P. *Journal of Polymer Science: Part B: Polymer Physics* **1998**, 36-45, 2025.

3. Barrer, R. M.; Barrie, J. A.;Slater, J. *J. Polym. Sci.* **1958**, 27, 177-189.

4 . Bondar, V. I ; Kamiya, Y. *J. Polym. Sci.: Part B : Polym. Phys.* 34, 369-379.

5 . Sanchez, I. C.; Lacombe, R. H. *The journal of Physical Chemistry* **1976**, 80, 2352-2360.

6. Condo, P.D.; Sanchez, I. C.; Panayiotou, C.G.; Johnston, K.P. *Macromolecules*, **1992**, 25, 6119-6129.

7. DiMarzio, E.A.; Gibbs, J.H.; Flemin, P.D.; Sanchez. I.C. *Macromolecules* **1976,** 9, 763-772.

8. Wissinger , R. G; Paulaitis, M. E. *Ind. Eng. Chem. Res.* **1991,** 30, 842-851..

9. Liu, D. ; Li, H.; Noon, M. S.; Tomasko D. L. *Macromolecules* **2005** 38, 4416 –4424.

10. Doghieri, F.; Sarti, G. C. *Macromolecules* **1996**, *29, 7885-7896.*

11. Chen, K. J.; Rizyi, S. S. H. *Journal of Polymer Science: Part B: Polymer Physics* **2006,** 44, 607-621.

12 . Cusarino P.; Brunacci A.; Pedemontea E. *Macromol. Chem. Phys.* **1996,** 197, 3773-3782.

13 Chllaghan, T. A. ; Paul, D. R. *Macromolecules* **1993**,*26, 2439-2450.*

14. Qiu, Z. Komura, M.; Ikehara, T. Nishi, T.*Polymer* **2003,** 44, 8111-8117.

15. Nishi, T. ; Wang, T.T. *Macromolecules* **1975,** 8, 909-915.

16. Condo, P.D. Ph. D. Dissertation , USA: The University of Texas at Austin, **1993**, 1-44.

17. Sato, Y.; Yamane, M.; Sorakubo, A.; Takishima, S.; Masuoka, H; Yamamoto, H.; Takasugi M. *The 21st Japan Symposium on Thermophsical Properties*, Nagoya, Japan, **2000**, 196-199.

18 . X. Hu, A.V. Nawaby. H. E. Naguib, M. Day, X. Liao, *ANTEC*, **2005**, Boston, USA.

19. Honda, Y. P.; Zhang, Z. *Journal of Polymer Science: Part B: Polymer Physics* **2000,** 38, 716-725.

20. Gendron, R. (editor), *Thermoplastic Foam Processing: Principles and Development (Polymeric Foams Series)*, CRC Press: USA, **2005**, 31-32

Chapter 5

Conclusions and Recommendations

5.1 Conclusions

PLLA/PMMA blends with all compositions (75/25%50/50% 75/25%) prepared by melt mixing showed only one T_g in DSC analysis and no phase separation was found. Heat induced crystallization was found in blends with PLLA composition larger than 50 wt% at the experimental temperature. However, CO_2-induced crystallization was also observed in samples above certain saturation pressures for all blends. Furthermore, addition of PMMA in blends reduced the kinetic process of crystallization and raised the decomposition temperature. The decomposition rate of blends was found to be highly dependent on composition.

High saturation pressures and lower saturation temperature resulted in similar levels of CO_2 dissolution in the blends. However, the Henry's law constant for CO_2 in the blends was found to increase with an increase in PLLA composition thus strongly suggesting an increase in the free volume of the samples. This observation was further supported by the DSC results obtained and the shift in the glass transition temperature to lower values. The diffusion coefficients were also found to be concentration dependent and as such a very strong indication of phase transitions occurring in the polymer-gas system at 25°C and 0°C. The sharp increases observed in the diffusion coefficients were indicative of the existence of the retrograde behavior in the blends. The changes in the diffusion coefficients as observed very much resembled the behavior in diffusion

coefficients as a function of gas pressure in PMMA-CO_2 system whereby the existence of the retrograde behavior was first reported through mathematical calculations.

A model based on lattice fluid theory, solution equilibrium theory and Gibbs-Di Marzio dynamic criterion was adopted to predict the CO_2 solubility, swelling factor and glass transition behaviors in PLLA/PMMA-CO_2 system. The mismatch between the predicted CO_2 solubility and experimental values was thought to be as a result of phase transitions and polymer swelling during the sorption process. Nevertheless, retrograde behavior in the PLLA/PMMA-CO_2 system was successfully predictable using this model.

Finally, micro cellular foams were produced by solid state foaming process in this study. Foams produced from higher saturation pressure at 25°C resulted in lower foam densities. With addition of PMMA to PLLA an improvement on the foam morphologies were observed and by decreasing the saturation pressure to 0°C from 25°C morphologies with open and interconnected pores were created. These morphologies thus have the potential to be used as scaffolds in biomedical applications.

5.2 Recommendations

In order to study the influence of foaming conditions on foam properties, the foaming experimental conditions need to be improved and a wider temperature and pressure range must be considered. Furthermore, given the time lines of this project it was impossible to conduct mechanical studies on the prepared porous materials. As such mechanical properties of blends and their foams are parameters needed to be studied in order to find the proper applications of the PLLA/PMMA blends.

Finally, more experimental CO_2 solubility data in rubbery state are needed for the theoretical model. The predicted swelling factors and glass transition behaviors for blends will also have to taken into consideration for correction of data.

Appendix A

Java Program

```
/* This program calculates the glass transition temperature as function of pressure in Polymer-Gas System.
The program was originally written in FORTRAN 77 by Dr. Condo was transferred partly, recoded to
JAVA by Baisheng Yao and was used to predict the effects of gas on the glass transition profile of polymer
blends. */

 import java.io.*;
 import java.lang.Math;
 import java.util.ArrayList;
 import java.lang.reflect.Array;


public class Poly_Gas_Tg {
         public static double R=8.314;
        //CO2 Data Mw-molar weight, T(K), P(pa), critical temperature, D(kg/cm-3)
         public static double Mw1=44.01, Tc1= 308.64, Pc1=574000000.0, Dc1=1505.0;

          /* PMMA Data Data Mw-molar weight, T(K), P(pa) critical temperature  entheropy of PMMA
               (J/mol)*/
           //public static double  Z=5.0, ZETA12=1.153, AX12=1.000, S1S2=1.000;// interaction data
           //public static double Mw2=108500.0, Tc2=696.0, Pc2=503000000.0,
               Dc2=1269.0,E2=7442.99988;

           // PLLA
           public static double  Z=5.0, ZETA12=1.141, AX12=1.000, S1S2=1.000;
           public static double Mw2=63366.0, Tc2=631.0, Pc2=559200000.0, Dc2=1333.0,E2=6335.6;

          //PLLA25%
          //public static double  Z=5.0, ZETA12=1.138, AX12=1.000, S1S2=1.000;
          //public static double Mw2=97217, Tc2=668.9, Pc2=523100000.0, Dc2=1284.4, E2=7075.7;

          //PLL50%
          //public static double  Z=5.0, ZETA12=1.131, AX12=1.000, S1S2=1.000;
          //public static double Mw2=85933, Tc2=651.6, Pc2=538200000.0, Dc2=1300, E2=6764.3;

           //PLLA 75%
          //public static double  Z=5.0, ZETA12=1.137, AX12=1.000, S1S2=1.000;
         //public static double Mw2=74649, Tc2=639.7, Pc2=549900000.0, Dc2=1316.4, E2=6525.0;

  // Constant Value
   public static double R1=(Mw1*Pc1)/(R*Tc1*Dc1)/1000.0;
   public static double R2=(Mw2*Pc2)/(R*Tc2*Dc2)/1000.0;
  //characteristic mer volume of compontnents
   public static double V1S=(1.0/ (Dc1*R1))*(Mw1/1000.0);
   public static double V2S=(1.0/ (Dc2*R2))*(Mw2/1000.0);
   public static double[] P=new double[2000];// Pressure array
   public static double[] T=new double[2000];// Temperature  array

   // give the start end value of P, T;
```

```
public static double  startP=26;
public static double  endP=24;
public static double  startT=50;
public static double  endT=10;
public static double  P_step=0.1,T_step=1;// iterate step distance for T, P

// method for calculation Reduced Density
public double calculateDensity (double D_start, double R, double P_R, double T_R ){
     int it=10000;
     double D_mid=1-Math.exp(((-Math.pow(D_start,2.0)- P_R)/T_R)+ D_start*(1/R-1));
     do {D_start=D_mid;
       it--;
       if (it<1)
          return 0.0000;
        else {D_mid=D_mid=1-Math.exp(((-Math.pow(D_start,2.0)- P_R)/T_R)+ D_start*(1/R-1));}}
     while(Math.abs((D_mid-D_start)/D_mid)>=0.000001);
    //System.out.println("D="+D_mid);
     return D_mid;
     }

// method for calculation reduced parameters TMXR,PMXR,PHI2PR,V12S, X12, VMXS;
 public double[] reduce(double PHI1, double Tj, double Pi ){
          double E11S=Tc1*R, E22S=Tc2*R;
          double[] T_PMXR=new double[20];
          double PHI2=1.0-PHI1,  RMX=1.0/((PHI1/R1)+(PHI2/R2));
       double Xl=(PHI1*RMX)/R1, X2=1.0-Xl;
       double PHI2PR=PHI2/(PHI2+(PHI1*S1S2));
       double E12S=ZETA12*(Math.sqrt(E11S*E22S));
       double X12=(E11S+(S1S2*E22S)-2.0*(Math.sqrt(S1S2))*E12S)/(R*Tj);
       double EMXS=(PHI1*E11S)+(PHI2*E22S)-(PHI1*PHI2PR*X12*R*Tj);
       double V12S=AX12*Math.pow((((Math.pow(V1S,1.0/3.0))+(Math.pow(V2S,1.0/3.0)))/2.0),3.0);
       double VMXS=(Math.pow(PHI1,
2.0)*V1S)+(2.0*PHI1*PHI2*V12S)+(Math.pow(PHI2,2.0)*V2S);
       double TMXS=EMXS/R,PMXS=((R*TMXS)/VMXS);
       double TMXR=Tj/TMXS,PMXR=Pi/PMXS;
  // add data to return array and pass to next calculate reduced Mix density, chem U.
        T_PMXR[0]=TMXR;
        T_PMXR[1]=PMXR;
        T_PMXR[2]=PHI2PR;
        T_PMXR[3]=V12S;
        T_PMXR[4]=X12;
        T_PMXR[5]=VMXS;
        T_PMXR[10]=RMX;
            T_PMXR[11]=Xl;
            return T_PMXR;
       }

   //      calaculate MixchemU and  reach the equlirium by iterate PHI1, MixtureDensity,
         public double [] MixChemU(double phi1, double[] t_pxr,  double mixd, double u0, double T1R
,double Tj,
                              double Pi, ArrayList Tj_PHI1_MixD_MixU_TPMXR_List) {
                  double PHI1=phi1, MixD=mixd, U0=u0;
                  double[] T_PMXR=t_pxr;
                  double diffLast=0;;
                  double diff ,mixU, PHI2=1-PHI1;
                  double Tj_PHI1_MixD_MixU_TPMXR_array[]= new double[10];
```

```
        do {
                mixU=Math.log(PHI1)+PHI2*(1.0-
(R1/R2))+R1*MixD*T_PMXR[4]*(Math.pow(T_PMXR[2],2.0));
          mixU=mixU+(R1*((1.0/MixD)-1.0)*Math.log(1.0-MixD))+Math.log(MixD)-((R1*MixD)/T1R);
          double TERM30=(R1*T_PMXR[1])/(T_PMXR[0]*MixD);
          double TERM31=(((2.0*PHI1*V1S)+(2.0*PHI2*T_PMXR[3]))/T_PMXR[5])-1.0;
          mixU=mixU+(TERM30*TERM31);
          diff=mixU-U0;
          if(diffLast*diff<0){
                Tj_PHI1_MixD_MixU_TPMXR_array[0]=Tj;
          //    System.out.println("********"+Tj);
                Tj_PHI1_MixD_MixU_TPMXR_array[1]=PHI1;
                Tj_PHI1_MixD_MixU_TPMXR_array[2]=MixD;
                Tj_PHI1_MixD_MixU_TPMXR_array[3]=mixU;
                Tj_PHI1_MixD_MixU_TPMXR_array[4]=U0;
                Tj_PHI1_MixD_MixU_TPMXR_array[5]=T_PMXR[0];
                Tj_PHI1_MixD_MixU_TPMXR_array[6]=T_PMXR[1];
          }
          PHI1=PHI1+0.0001;
          diffLast=diff;
          T_PMXR=reduce(PHI1, Tj, Pi);
          MixD=calculateDensity (0.9999, (R1)/PHI1, T_PMXR[1], T_PMXR[0] );
       }while(PHI1<1.0);
      // System.out.println("********");
       Tj_PHI1_MixD_MixU_TPMXR_List.add(Tj_PHI1_MixD_MixU_TPMXR_array) ;
          return Tj_PHI1_MixD_MixU_TPMXR_array;
          }


    //calculate Tg
    public ArrayList CalTg (ArrayList  Tj_PHI1_MixD_MixU_TPMXR_List) {
        ArrayList S_Tg_List=new ArrayList();
        double[] Tj_array=new double[Tj_PHI1_MixD_MixU_TPMXR_List.size()];
        double[] S_array=new double[Tj_PHI1_MixD_MixU_TPMXR_List.size()];
        double[] S_original_array=new double[Tj_PHI1_MixD_MixU_TPMXR_List.size()];
        double Tj, PHI1, mixD, Xl, X2, S1, diff, diffLast=0;

          for (int i=0; i<Tj_PHI1_MixD_MixU_TPMXR_List.size(); i++ ){

                Tj=((double[]) Tj_PHI1_MixD_MixU_TPMXR_List.get(i))[0];
                PHI1=((double[]) Tj_PHI1_MixD_MixU_TPMXR_List.get(i))[1];
                mixD=((double[]) Tj_PHI1_MixD_MixU_TPMXR_List.get(i))[2];
                double PHI2=1.0-PHI1;
                double RMX=1.0/((PHI1/R1)+(PHI2/R2));
                Xl=(PHI1*RMX)/R1;
                X2=1.0-Xl;
                double A=(Z-2.0)*Math.exp(-E2/(R*Tj));
          double F2=(A/(1.0+A));

       //Item5 Not Match With Thesis
       double  item1=-RMX*((1.0-mixD)/mixD)*Math.log(1.0-mixD);
       double  item2=-((Xl*Math.log(Xl))+(X2*Math.log(X2)));
       double  item3=Xl*(R1-2.0)*Math.log(Z-1.0);
       double  item4=X2*(R2-2.0)*(((F2*E2)/(R*Tj))-Math.log(1.0-F2));
       double  item5=1-Math.log(mixD)-RMX+Math.log(Z*RMX/2);
         S1=item1+item2+item3+item4+item5;
```

```
        S1=S1/X2;
        Tj_array[i]=Tj;
        S_array[i]=S1;
        S_original_array[i]=S1*X2;
        diff=S1-diffLast;
        diffLast=diff;
          }

      S_Tg_List.add(Tj_array);
      S_Tg_List.add(S_array);
      S_Tg_List.add(S_original_array);
      return S_Tg_List;

}
   // method for parse Tg  after got all data( from return list ) and out put to file3
   public void parseTg(ArrayList S_Tg_Arraylist, PrintWriter f3, double P)  {

        double[] Tj=new double[10000];
        Tj=(double[])(S_Tg_Arraylist.get(0));
        double [] S =new double[10000];
        S=( double[])(S_Tg_Arraylist.get(2) );
        boolean  flag=true;

        double Tmin=0.0;
        double t_step=0.0;
   //   double TgTemp=0, TgTemp2=0;
        f3.println();
    //  f3.println("Please refer file2 to decide the Tg, Tg is related the step precision of you chose  " );
        f3.println(" P(atm) = "+ Double.parseDouble
                                (new java.text.DecimalFormat("##.##").format(P/1.01325E5)));
     //int flag2=0;
        for (int i=1; i<(int)Array.getLength(Tj); i++){
        //        find mimum value in s point
                Tmin=Tj[i];

              // System.out.println("Tj="+Tj[i-1]+"  S="+S[i-1]);

                                if((Math.abs(S[i-1]))<(Math.abs(S[i]))){

                                  Tmin=Tj[i-1];
                                 //  Smin=S[i-1];
                                  flag=false;

                                  }


            // look for value near 0
                    if ((S[i]*S[i-1]<0)){
                   t_step=Tj[i]-Tj[i-1];
                   //       System.out.println("Tmin="+Tmin+", i= "+i);

                  //System.out.println("t_step="+t_step+" Math.abs(S[i-1])/Math.abs(S[i-1]-
S[i])="+Math.abs(S[i-1])/Math.abs(S[i-1]-S[i]));
                  // System.out.println(" Math.abs(S[i-1]-S[i])="+Math.abs(S[i-1])/Math.abs(S[i-1]-S[i]));

                   if (flag)
```

```
                                    Tmin=Tmin-t_step*(Math.abs(S[i])/Math.abs(S[i-1]-S[i]));
                                   else
                                    Tmin=Tmin+t_step*(Math.abs(S[i-1])/Math.abs(S[i-1]-S[i]));

                                            f3.println(" Tg(K) = "+ Double.parseDouble
                                  (new java.text.DecimalFormat("##.##").format(Tmin)));
                                  //Temp=Tmin;

                                   System.out.println("Tg="+new
java.text.DecimalFormat("##.##").format(Tmin) );
                                  }

                      flag=true;
                     }


            }



 // main function
  public static void main(String[] args) throws IOException {

  PrintWriter f2=new PrintWriter
                                  (new FileWriter("file2.text"));// record Tj,  PHI1,Mix reduced density
after set  Umix=U0
  PrintWriter f3=new PrintWriter
                                  (new FileWriter("file3.text"));// record Tg by set entropy  to 0
  f3.println("Please refer file2 to decide the Tg, Tg is related the step precision of you chose  " );

  // for (int i=0;i<=5; i++){
  for (int i=0;i<=(int)((startP-endP)/P_step); i++){
             ArrayList S_Tg_Arraylist=new ArrayList();
             Poly_Gas_Tg PolyTg=new Poly_Gas_Tg();// iniciate a object for process
          double P1_R, P2_R,T1_R,T2_R;// ratio of P T
      double gasReducedD, polyReducedD, mixReducedD, pureChemU;
      double  PMXR, TMXR, PHI2PR, V12S, X12;// variable in calculation
          double[] T_PMXR_Array=new double[20]; // return array  from reduce which record T_MXR,
P_MXR,
      double[] Tj_PHI1_MixD_MixU_TPMXR_array=new double[10];// return array  after reduce MiX
density which record MixDensity, PHI1, T_MXR, P_MXR,
      ArrayList Tj_PHI1_MixD_MixU_TPMXR_List= new ArrayList(); //hold return
Tj_PHI1_MixD_MixU_TPMXR_array after  serials Tj
      double PHI1 =0.0;

      P[i]=(startP-P_step*i)*(1.01325E5);
      P1_R=P[i]/Pc1;
      P2_R=P[i]/Pc2;
      System.out.println();
      System.out.println("P="+P[i]/1.01325E5);

      for (int j=0; j<=(int)((startT-endT)/T_step); j++){
           T[j]=startT-T_step*j+273.15;
        //  System.out.println("qqqqT"+j+"="+T[j]);
          T1_R=T[j]/Tc1;
           T2_R=T[j]/Tc2;
```

```
        gasReducedD=PolyTg.calculateDensity (0.0001, R1, P1_R, T1_R );// gas density

        polyReducedD=PolyTg.calculateDensity (0.9999, R2, P2_R, T2_R );// polymer density
       // calculate Pure chem U
        pureChemU=(R1)*((1.0-gasReducedD)/gasReducedD)*Math.log(1.0-
gasReducedD)+Math.log(gasReducedD)
              -(R1)*(gasReducedD)/T1_R+(R1)*P1_R/(T1_R*gasReducedD);

        //ALCULATE REDUCED PARAMETERS FOR POLYMER-RICH PHASE PMXR, TMXR
        // problems for PHI1 in hear  System.out.println("PHI11="+ PHI1+",   temp=");

        T_PMXR_Array=PolyTg.reduce(PHI1, T[j],P[i]);
        TMXR=T_PMXR_Array[0];
        PMXR= T_PMXR_Array[1];
        PHI2PR=T_PMXR_Array[2];
        V12S=T_PMXR_Array[3];
        X12=T_PMXR_Array[4];

    //    System.out.println("PHI11="+ PHI1+",   temp=");
    //    System.out.println("R1/PHI1="+ R1/PHI1+",   temp=");
        // Mixture reduced density
        mixReducedD=PolyTg.calculateDensity (0.9999, (R1)/PHI1, PMXR, TMXR );
        // adjust PHI1,MixD MixU TPMXR make MixChemU=pureChemU;
        Tj_PHI1_MixD_MixU_TPMXR_array=PolyTg.MixChemU(PHI1, T_PMXR_Array,
mixReducedD,
                    pureChemU, T1_R, T[j], P[i], Tj_PHI1_MixD_MixU_TPMXR_List );

                    }//T circulation
                    // calculate Tg by entrophy=0
                    S_Tg_Arraylist=PolyTg.CalTg ( Tj_PHI1_MixD_MixU_TPMXR_List) ;
      // out put to file2
      f2.println("P(atm)="+Double.parseDouble
                      (new java.text.DecimalFormat("##.#####").format(P[i]/1.01325E5))+",   ");
                    f2.println("Tj(K)    "+"PHI1  "+ "MixD(g/cm-3)  "+"MixU/RT    " + "U0/RT    "
+"S/R    " );
      for( int k=0; k<Tj_PHI1_MixD_MixU_TPMXR_List.size(); k++){
                     double[] array1= (double[]) Tj_PHI1_MixD_MixU_TPMXR_List.get(k);
                              double[] array2= (double[]) S_Tg_Arraylist.get(2);
                              for(int l=0; l<5; l++){
                             f2.print(Double.parseDouble
                              (new java.text.DecimalFormat("##.####").format(array1[l]))+",   ");
                          }
                          f2.print(Double.parseDouble
                         (new java.text.DecimalFormat("##.####").format(array2[k]))+",   ");
                          f2.println();
                     }
                    //Parse Tg and output to file3
      PolyTg.parseTg(S_Tg_Arraylist, f3, P[i]);
   } //// P circulation
         f2.close();
   f3.close();
 }//main finished
}
```